1116

Study on the improvement of drift behavior and packaging of pH-ISFETs

Dissertation
submitted to the Faculty of Sciences of the University of Neuchâtel,
to obtain the degree of Doctor of Sciences

by

胡 波

HU Bo

Dipl. Informatique
Computer Science department
Beijing Polytechnic University, P. R. China

Institute of Microtechnology
University of Neuchâtel
Breguet 2, CH-2000 Neuchâtel
Switzerland

27 March 1991

printed by Drukkerijen Nederland b.v.
Enschede, The Netherlands
July 1991

IMPRIMATUR POUR LA THÈSE

Study of Improvement of Drift Behavior and Packaging of ISFETs

de M. Bo Hu

UNIVERSITÉ DE NEUCHÂTEL

FACULTÉ DES SCIENCES

La Faculté des sciences de l'Université de Neuchâtel
sur le rapport des membres du jury,

Messieurs N. de Rooij, A. Shah, M. Decroux (Genève) et P. Bergveld (Twente)

autorise l'impression de la présente thèse.

Neuchâtel, le 18 juin 1991

Le doyen :

Cl. Mermod

献给

我亲爱的

父母，妻子，儿子。

to my parents
my wife
my son

Contents

CHAPTER 1
Introduction

CHAPTER 1 Introduction

1.1 Introduction

Great importance has been attached, worldwide to the applications of chemical sensors in the field of biomedicine. One of the most important and commonly used of these sensors is a device based on the field effect transistor which is the Ion Sensitive Field Effect Transistor (ISFET). Since the first ISFET was presented by Bergveld in 1970 [1], many investigations on the theory, various fabrications and applications of the ISFETs have been reported [2-5]. The characteristics of pH-ISFETs with different pH sensitive materials have been investigated on the following basis, pH sensitivities [3,5,6], temperature sensitivity [3,7,8] and long term drift [6,9,10,11]. From these studies some of the main problems due to packaging, drift and temperature sensitivity were found. The packaging problems previously prevented a widespread application of biochemical and integrated sensors. One possible solution is to use back-side contacts on the device chips. These have applications in the measurement of interdental plaque pH with a pH-ISFET encapsulated in the dental prosthesis, and an integrated pressure-pH sensor on one chip [12,13, 14]. The appearance of the ISFET with back-side contacts also allows the ISFET to be used as a pH sensitive element in the gas sensitive sensors. In chapters 3 and 4 the ISFET with back-side contacts and its application in the CO_2 sensor based on Severinghaus principle [15] are presented.

In the cases where high accuracy and continuous measurement are needed, the long term drift has to be taken into account as it impedes the application of the ISFET. Therefore, in this thesis the drift behavior and different approaches for reducing drift rate of the pH-ISFET, using alumina as pH sensitive layer, are discussed. These approaches include fabrication techniques and measuring methods. In order to reduce the drift effect with differential measurement using an ISFET-MAOSFET pair, a previous investigation of distribution of the ΔV_T of dual FETs was done and is also discussed in this thesis.

Another interesting investigation, showing us that the pH sensitive mechanism of the Al_2O_3 ISFETs, is based on the surface potential due to interaction on the solid/liquid interface [16,17]. According to this theory the temperature dependence of the surface potential had been further studied [11,18]. In this study it was found that the temperature response of the ISFET varied with the pH of the solution. Taking into account the pH temperature dependence of the solution, this response had a constant sensitivity. This gave us the idea to create a new system for determining the pH of solution. In principle, using this technique the drift of the ISFET can be eliminated. This new technique for determination of pH, using ISFETs, is presented in this thesis.

1.2 Outline of this thesis

In chapter 2, ISFET theory is discussed using the theory of the IGFET (Insulator Gate Field Effect Transistor) as the background. The derivation of the basic characteristics of ISFET and experimental results for these characteristics, such as pH sensitivity, temperature sensitivity and drift behavior is given, thus allowing an understanding of the functions of the ISFET and the problems in its applications.

Chapter 3 presents an ISFET and a combined pH/Temperature sensor with back side contacts. The fabrication techniques for making back-side contacts are explained. This contact technique overcomes some of the difficulties in the encapsulation and bonding processes for the specific requirement.

Chapter 4 gives an example of the application of a pH-ISFET with back-side contacts. A CO_2 sensor based on the Severinghaus principle, using an ISFET as the pH sensing element is presented. The characteristics of the sensor and their measuring results are shown and discussed.

Chapter 5 presents a novel measurement technique based on the temperature modulation of ISFETs. Using this technique the long term drift of ISFET can be eliminated and prove again that the long term drift of ISFETs with alumina as the pH sensitive layer is caused by solid state effects theoretically and practically.

Chapter 6 discusses the reduction of the long term drift of the ISFET with a processing of the alumina deposition with low hydrogen content and an additional anneal with aluminum over the gate of the ISFET.

The influence of the distribution of differential pairs of ISFET and MAOSFET over a wafer are discussed in Chapter 7.

Chapter 8, finally, summarizes the conclusions of this work.

1.3 References

[1]. P. Bergveld, IEEE Trans. Biomed. Eng., Vol. BME-17, 1970, 70-71.

[2]. P. Bergveld, IEEE Trans. Biomed. Eng., Vol. BME-19, 1972, 342-351.

[3]. P.W. Cheung, W.H. Ko, D.J. Fung and S.H. Wong, CRC Press. 1978, 1978, 91-117.

[4]. J. Janata and R.H. Huber, in H. Freiser (Ed.): Ion-selective electrodes in analytical chemistry II, Plenum Press., 1980, 107-174.

[5]. H.H. van den Vlekkert and N.F. de Rooij, Analysis, Vol. 16, No. 2, 1988, 110-119.

[6]. H.Abe, M. Esashi and T. Matsuo, IEEE Trans. Electron Devices, Vol. ED-26, No. 12, 1979, 1939-1944.

[7]. O. Leistiko, Physica Scripta, Vol. 18, 1978, 445-450

[8]. G.H. Wang, D. Yu and Y.L. Wang, Sensors and Actuators, Vol. 11, 1987, 211-237.

[9]. H.C.G. Ligtenberg, Thesis, University of Twente, The Netherlands, 1987.

[10]. C. Arnoux, Thesis, University of Neuchâtel, Switzerland, 1988.

[11]. H.H. van den Vlekkert, Thesis, University of Neuchâtel, Switzerland, 1988.

[12]. J.C.-M. Huang and K.D. Wise, IEEE IEDM 82, 1982, 316-319.

[13]. H.H.van den Vlekkert, B. Kloeck, D.Prongue, J. Berthoud, B. Hu, N.F. de Rooij, E. Gilli and Ph.de Crousaz, TRANSDUCERS '87, TOKYO, Japan, 1987, 726-729.

[14]. H.H.van den Vlekkert, B. Kloeck, D.Prongue, J. Berthoud, B. Hu, N.F. de Rooij, E. Gilli and Ph.de Crousaz, Sensors and Actuators Vol. 14, No. 4, 1988, 165-176.

[15]. J. W. Severinghaus and A. F. Bradley, J. Appl. Physiol. 13 (1958), 515-520.

[16]. G.A. Bootsma, N,F. de Rooij and A van Silfhout, Sensors and Actuators, Vol. 1, 1981, 111-136.

[17]. L. Bousse, N.F. de Rooij and P. Bergveld, IEEE Trans. Electron Devices, Vol. ED-30, No. 10, 1983, 1263-1270.

[18]. H.H. van den Vlekkert, L. Bousse and N. de Rooij, J. Colloid and Interface Science, Vol. 122, No. 2, 1988, 336-345.

CHAPTER 2
The Characteristics of ISFET

CHAPTER 2 The Characteristics of ISFET

2.1 Abstract

The characteristics of pH sensitivity, temperature response and the baseline drift of ISFETs using alumina as the pH sensitive material are discused in this chapter. A pH sensitivity of about 55 mV/pH and a long term drift of less than 0.2 mV/h after 10 hours in a buffer solution show a possibility to apply such miniaturized chemical sensor to the biomedical field.

2.2 Introduction

Miniaturized silicon sensors for biomedical applications have received considerable attention for several years. The appearance of the first ISFET (Ion Selective Field Effect Transistor) presented by Bergveld in 1970 [1] has created a new investigation field for chemical sensors. Compared to similar sensors, such as glass electrodes ISFET has the following specific advantages: small size, the possibility of making multi-ion sensors, integration of signal processing capabilities. Moreover since the development of membranes for specific ions, the ISFETs are not only suitable in the field of chemical sensors but also for biochemical and biomedical sensors, for example, to detect penicillin [2] and glucose [3]. An integrated microelectronic solid state technology is used in fabrication of the ISFET, miniaturization and mass production of the sensors at a low cost is made easy.

The ISFET can be considered as an IGFET (Insulated Gate Field Effect Transistor) where the metal gate is replaced by a reference electrode, electrolyte solution and an ion-selective material deposited over the gate insulator, as is shown in Figure 2-1.

The different ion-selective materials determine the applications of the ISFETs, for example inorganic insulators such as Si_3N_4, Al_2O_3 and Ta_2O_5 are pH sensitive materials [4,5], and aluminosilicates are pNa or pK sensitive materials [5,6]. In order to understand the ISFET, the characteristics of the ISFET will be discussed in this chapter. The pH-ISFET is used as an example.

2.3 The IGFET

IGFET theory is based on the analysis of the Metal Insulator Semiconductor (MIS) structure. Consider the cross-section and the related energy band diagrams of the MIS structure, as is shown in Figure 2-2 and Figure 2-3.

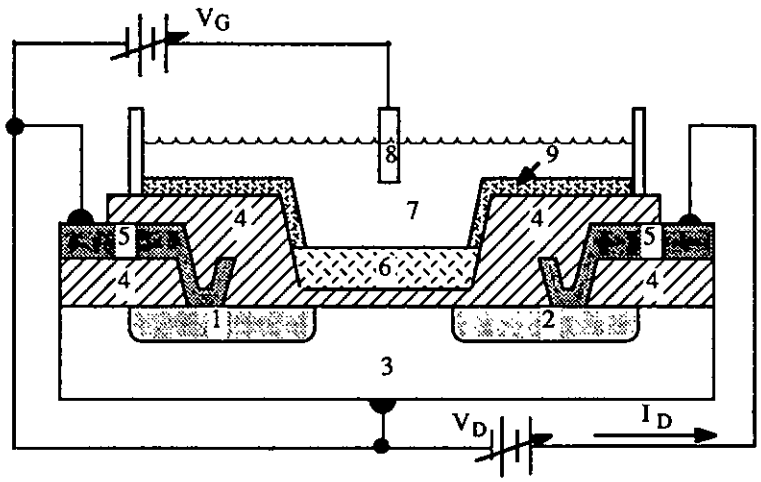

Figure 2-1. *Schematic diagram of the ISFET. (1) source, (2) drain, (3) p-type silicon substrate, (4) SiO_2 insulator, (5) Al contacts, (6) membrane, (7) electrolyte solution, (8) reference electrode and (9) encapsulant.*

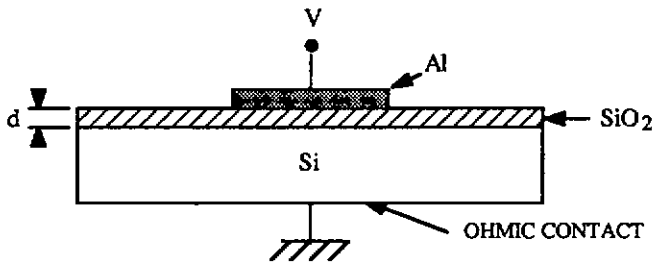

Figure 2-2. *Cross section of the MIS structure.*

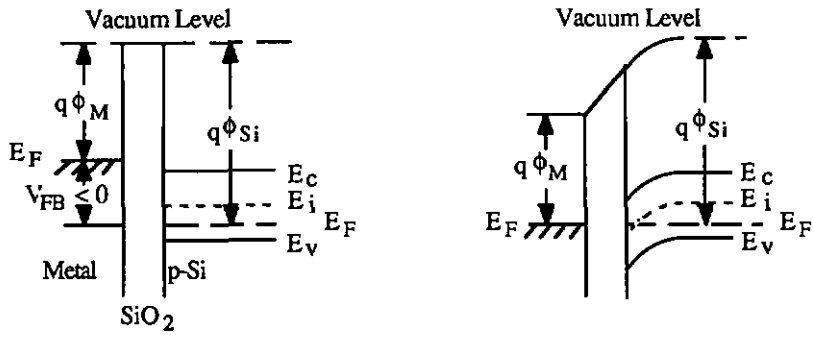

Figure 2-3. *(a)Energy band diagram of the MIS in flat-band condition. (b) Energy band diagram of the MIS in thermal equilibrium.*

In order to bring about thermal equilibrium, a charge flow takes place between the metal and the semiconductor. This results in band bending at the semiconductor surface when no external voltage is applied to the gate, as is shown in Figure 2-3(a). A nonzero work function difference (ϕ_{MS}) is created between the metal work function (ϕ_M) and the semiconductor work function (ϕ_{Si}). A gate voltage equal to ϕ_{MS} is required to bring about the flat-band condition shown in Figure 2-3(b). It is called the flat-band voltage V_{FB}. In the absence of any additional charge in the insulator, V_{FB} is equal to the difference of the work functions:

$$V_{FB} = \phi_M - \phi_{Si} = \frac{1}{q}\Phi_M - \frac{1}{q}\Phi_{Si} = \phi_{MS} \qquad (2\text{-}1)$$

The gate voltage necessary to achieve the flat-band condition is further modified by charges residing within the insulator. These charges will induce charges in both the metal and the semiconductor. The induced charges on the surface of the semiconductor will again result in band bending at the surface even for the condition of no externally applied voltage. Consequently V_{FB} has to be rewritten as:

$$V_{FB} = \phi_{MS} - \frac{Q_{ss}}{C_o} \qquad (2\text{-}2)$$

where Q_{ss} is the charge in the insulator per unit area and C_o the insulator capacitance. The insulator charge is composed of fixed charges Q_f and charges trapped in the surface states Q_{it}, both at the silicon/insulator interface, and of mobile charge Q_m existing due to the mobile ionic impurity distribution inside the insulator [7].

A voltage applied to the gate permitting band bending to decrease the difference between the intrinsic level E_i and the Fermi level E_F creates a depletion layer. If a large voltage is applied to the gate, the large band bending causes the intrinsic level E_i to cross over the Fermi level E_F at or near the surface of the semiconductor. The number of the minority carriers become greater than the number of majority carriers. Thus an inversion region is created at the surface, see Figure 2-4.

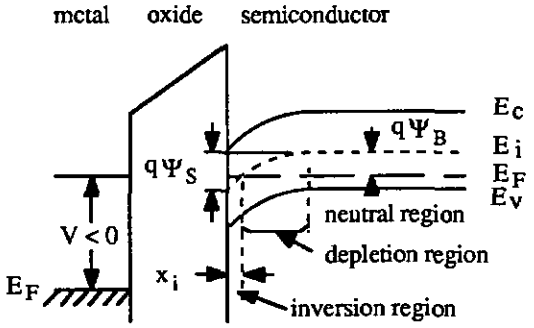

Figure 2-4. *Depletion and inversion region of the MIS structure.*

The surface depletion layer width reaches a maximum when the surface is strongly inverted. The required surface potential Ψ_S for strong inversion is:

$$\Psi_S = 2\Psi_B \tag{2-3}$$

The charge of the depletion layer is given by:

$$Q_B = - qN_A W_{depl.} = - \sqrt{2q\varepsilon_s N_A (2\Psi_B)} \tag{2-4}$$

where q is the unit charge, N_A is the doping density of the substrate, Ψ_B is the Fermi potential, ε_s is the semiconductor permittivity and $W_{depl.}$ is the width of the depletion layer that is expressed by:

$$W_{depl.} = \sqrt{\frac{2\varepsilon_s(2\Psi_B)}{q\ N_A}} \tag{2-5}$$

The applied voltage just sufficient to bring about strong inversion is called the threshold voltage V_T. It contains the voltage to achieve the flat-band condition and the term that is responsible for building up the strong inversion layer:

$$V_T = V_{FB} - \frac{Q_B}{C_o} + 2\Psi_B \qquad (2\text{-}6)$$

Figure 2-5 shows the typical construction and biasing arrangement for an n-channel IGFET. As a matter of fact the semiconductor substrate and metal gate form a parallel-plate capacitor. The V_G is applied between the substrate and the gate forming a MIS structure. The polarity and magnitude of V_G are such that the semiconductor field effect gives rise to an inversion layer on the surface of the p-type substrate under the gate. This n-type inversion layer forms a conducting channel between the source and drain regions. If a voltage V_D is applied to the drain with respect to the source and substrate, a current I_D passes through the channel connecting the drain and the source. The magnitude of the drain current I_D is determined by the electrical resistance of the surface inversion layer and the voltage difference V_D between the source and the drain.

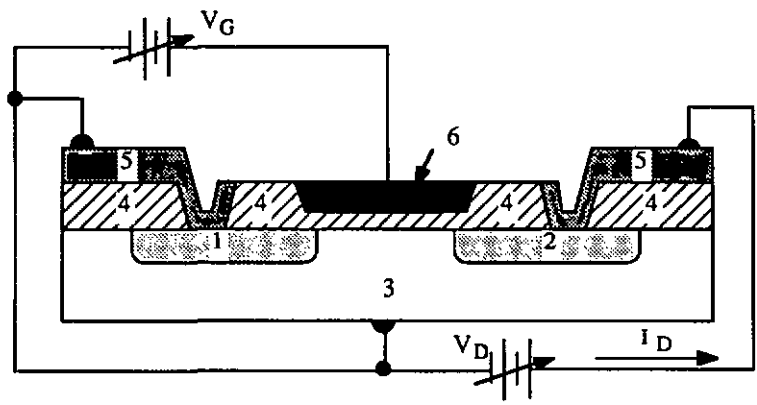

Figure 2-5. *Schematic diagram of the IGFET. (1) source, (2) drain, (3) p-type silicon substrate, (4) SiO_2 insulator, (5) Al contacts and (6) metal gate.*

The basis for the derivation of the current-voltage relationships is the calculation of the density of the mobile electrons in the surface inversion layer as a function of the applied voltages V_G and V_D, and position along the channel. The procedure of the derivation is discussed in detail by [8]. Two operation regions are distinguished. When $V_D < V_G - V_T$ the device works in the unsaturated region and the current-voltage relationship is expressed by:

$$I_D = \mu_n \frac{W}{L} C_o \left(V_G - V_T - \frac{1}{2} V_D\right) V_D \qquad (2\text{-}7)$$

where μ_n denotes the electron mobility,W the channel width and L the channel length. For $V_D > V_G - V_T$, the current is given by equation (2-7) with V_D replaced by $V_G - V_T$:

$$I_D = \mu_n \frac{W}{L} C_o \frac{(V_G - V_T)^2}{2} \qquad (2\text{-}8)$$

The changes of drain current with gate voltage corresponding to the IGFET characteristics expressed by equations (2-7) and (2-8) are shown in Figure 2-6.

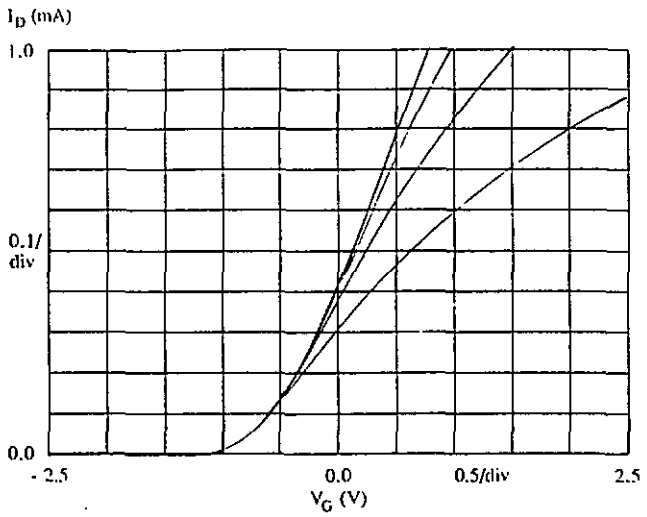

Figure 2-6. *The I_D-V_G characterisrics of an IGFET.*

2.4 The pH-ISFET

The ISFET shown in Figure 1 is different from the IGFET only on the gate area where the metal gate is replaced by a reference electrode, an electrolyte solution, and a sensitive material. This can be analyzed as an EOS (Electrolyte Oxide Semiconductor) structure, see Figure 2-7.

Considered as an electrochemical cell, the EOS structure is represented as:

metal (M) I Si I Insulator I Electrolyte I Reference electrode I metal (M')

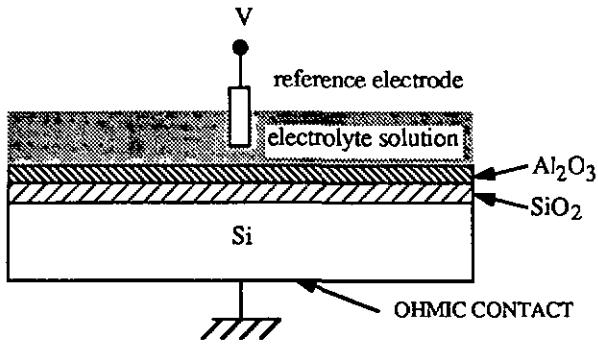

Figure 2-7. *Cross section of the EOS structure.*

In order to bring about the flat band condition, a voltage is externally applied on M'. This voltage is equal to the sum of the potentials situated on every interface. Thus, the flat band voltage for the ISFET may be derived as [9]:

$$V_{FB} = E_{ref} - \phi_{Si} - \Psi_o + \chi - \frac{Q_{ss}}{C_o} \qquad (2\text{-}9)$$

where E_{ref} is the reference electrode potential, Ψ_o the potential drop in the electrolyte at the insulator/electrolyte interface and χ the surface dipole potential of the solvent. Note that ϕ_M the metal work function of M' is already incorporated in E_{ref} and the variations of the potential χ is not included [9]. In order to account for the effect of the mobile charge in the insulator of the EOS structure, the distance d_c of this charge center to the insulator/electrolyte interface must be introduced. The insulator charge is expressed therefore as:

$$Q_{ss} = Q_f + Q_{it} + Q_m \frac{d_c}{d_i} \qquad (2\text{-}10)$$

The potential at the insulator/electrolyte interface Ψ_o mainly determines the response of the pH sensitive ISFET. The origin of this potential is the interaction of the insulator surface with ions present in the electrolyte solution. It is assumed that the surface of the insulator contains discrete surface sites. On the oxide surface the sites are in three possible forms: $A\text{-}O^-$, A-OH and $A\text{-}OH_2^+$. The acidic and basic character of the neutral site A-OH can be characterized by two equilibrium constants, K_a and K_b:

$$A\text{-}OH \Leftrightarrow A\text{-}O^- + H_s^+, \text{ with } K_a = \frac{[A\text{-}O^-][H^+]_S}{[A\text{-}OH]} \quad (2\text{-}11)$$

$$A\text{-}OH + H_s^+ \Leftrightarrow A\text{-}OH_2^+, \text{ with } K_b = \frac{[A\text{-}OH_2^+]}{[[A\text{-}OH][H^+]_S} \quad (2\text{-}12)$$

The equilibrium equations (2-11) and (2-12) have been derived from a statistical viewpoint by Healy and White [10]. In these equations $[H^+]_S$ represents the surface concentration of the H^+. Boltzmann statistics give the relationship between bulk and surface concentration as:

$$[H^+]_S = [H^+]_B \exp\left(-\frac{q\Psi_o}{kT}\right) \quad (2\text{-}13)$$

where k is the Boltzmann constant and T the absolute temperature. The concentration of the number of the surface sites N_S and the surface charge per unit area σ_o can be calculated by:

$$N_S = [A\text{-}O^-] + [A\text{-}OH] + [A\text{-}OH_2^+] \quad (2\text{-}14)$$

$$\sigma_o = q([A\text{-}OH_2^+] - [A\text{-}O^-]) \quad (2\text{-}15)$$

The preceding equations allow us to derive the relationship which is used to calculate the reactions which give rise to the surface potential Ψ_o at the interface. The derivation of the this equation has been discussed in detail by Bousse [9]. The equation is given by:

$$2.303\ (pH_{pzc} - pH) = \frac{q\Psi_o}{kT} + \sinh^{-1}\left(\frac{q\Psi_o}{\beta kT}\right) \quad (2\text{-}16)$$

where $pH_{pzc} = -\log_{10}\left(\frac{K_a}{K_b}\right)^{1/2}$ is the pH at the point of zero charge, ß is a dimensionless sensitivity parameter. Around the point of zero charge, the relation of the equation (2-16) can be linearized:

$$\Psi_o = \frac{\beta}{\beta+1}\frac{2.303kT}{q}(pH_{pzc}-pH) \quad (2\text{-}17)$$

This equation is only valid if $q\Psi_o/kT < \beta$ [9].

The threshold voltage V_T for the EOS is derived by substituting the equation (2-9) into equation (2-6):

$$V_T = E_{ref} - \phi_{Si} - \Psi_o + \chi - \frac{Q_{ss}}{C_o} - \frac{Q_B}{C_o} + 2\Psi_B \qquad (2\text{-}18)$$

Also the ISFET can be operated either in the unsaturated region or in the saturated region [8]. Using the same principle as for IGFET, the current-voltage relationships in two operating regions are derived similarly as the equations (2-7) and (2-8). The V_T in these equations should be replaced by expression (2-18). Figure 2-8 shows the result of the I_D-V_G characteristics for two pH values:

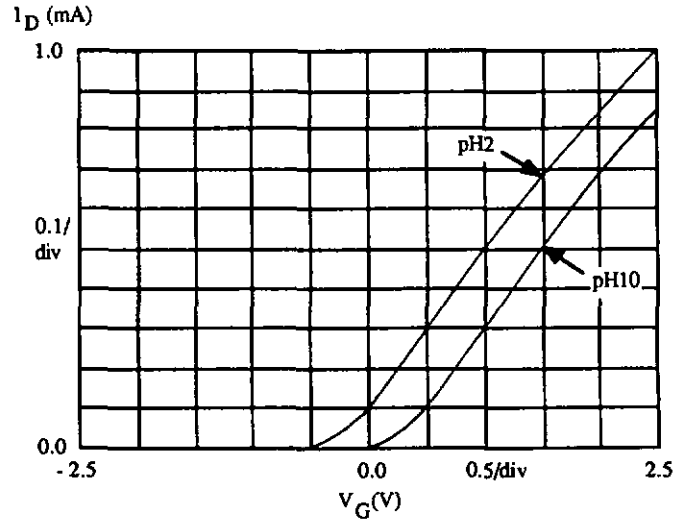

Figure 2-8. *The I_D-V_G characteristics of the ISFET for pH 2 and pH 10 values.*

2.5 Specific characteristics of the pH-ISFET

The constant current mode with constant V_D is often used as the operation mode of an ISFET. In this case, for the linear range, the V_G as a function of pH is derived from equation (2-7), where V_T is substituted by equation (2-18):

$$V_G = \frac{I_D L}{\mu_n W C_o V_D} + E_{ref} - \Psi_o + \chi - \phi_{Si} - \frac{Q_{ss}}{C_o} + 2\Psi_B - \frac{Q_B}{C_o} + \frac{1}{2} V_D \qquad (2\text{-}19)$$

From equation (2-17), V_G is seen to be dependent on pH, temperature T and time of exposure to the electrolyte solution t. The characteristics of the ISFET are obtained by developing V_G in a Taylor series at the point (pH_o,T_o,t_o), and taking into account only the first order terms. The pH sensitivity is expressed by:

$$\frac{\partial V_G}{\partial pH} = - \frac{\partial \Psi_o}{\partial pH} = 2.303 \frac{\beta}{\beta+1} \frac{kT}{q} \qquad (2\text{-}20)$$

The temperature sensitivity:

$$\frac{\partial V_G}{\partial T} = \frac{\partial V_T^{MOST}}{\partial T} + \frac{\partial E_{ref}}{\partial T} - \frac{\partial \Psi_o}{\partial T} - \frac{I_D\ L\ b}{\mu_n^o\ W\ Co\ T_o\ V_D} \qquad (2\text{-}21)$$

where μ_n^o is the electron mobility at the temperature T_o. The empirical relationship $\mu = aT^b$ for the electron mobility where a and b are constants independent of temperature is used [11,12]. V_T^{MOST} accounts for the threshold voltage of the solid state part of the sensor and is equal to threshold voltage of the IGFET minus the metal work function for the gate. The temperature dependence of V_T^{MOST} is given by the following expression [11,12]:

$$\frac{\partial V_T^{MOST}}{\partial T} = \frac{\partial \Psi_B}{\partial T}\left(2 - \frac{Q_B}{2\ C_o\ \Psi_B}\right) \qquad (2\text{-}22)$$

and

$$\frac{\partial \Psi_B}{\partial T} = -\frac{I}{T}\left(\frac{E_{go}}{2q} - \Psi_B\right) \qquad (2\text{-}23)$$

where E_{go} is the energy bandgap of the silicon at 0°C.

In first approximation, the drift behavior can be considered to be caused by the mobility of the charges at each interface between different materials over the gate and in the insulator, substrate and solution. These effects bring about changes, over time, in the threshold voltage of the solid state part and in the interface potential and the dipole potential. Assuming that E_{ref} is stable, the following relationship results:

$$\frac{\partial V_G}{\partial t} = \frac{\partial V_T^{MOST}}{\partial t} - \frac{\partial \Psi_o}{\partial t} + \frac{\partial \chi}{\partial t} \qquad (2\text{-}24)$$

2.6 Determination of the pH-ISFET characteristics

The pH-ISFET characteristics were measured on a n-channel ISFET with an alumina pH sensitive layer over the gate oxide. The fabrication process discussed in reference [13] was used. After the bonding and encapsulation of the ISFETs on supports, they were connected to a specially developed amplifier which operates the device at a constant drain current and a constant drain to source voltage. The V_G was the

experimentally determined quantity. The pH value of the solution was calibrated by a pH meter with a glass electrode and a reference electrode, and the temperature of the solution was measured at the same time.

pH sensitivity

A typical measurement for the pH sensitivity is shown in Figure 2-9 where V_G is plotted against pH. The pH value of a HCl-Tris buffer solution was varied between pH 2 and pH 10 by adding acid or base. The measurement was done at constant temperature and in the dark. The ISFET was operated at a drain current I_D of 100 μA and a drain voltage V_D of 0.5 V. A pH sensitivity of about 55 mV/pH was obtained.

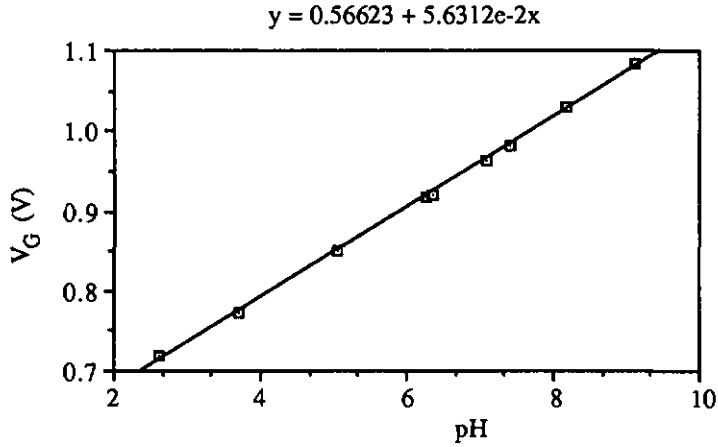

Figure 2-9. *The pH response of an ISFET at 25 °C.*

Temperature sensitivity

The temperature sensitivity was studied over the temperature interval 15-35 °C in the HCl-Tris buffer solution. Since the pH value of buffer solutions changes with temperature, the effect of the pH changes following temperature on the V_G should be taken into account. Therefore the measured result is given by:

$$\left(\frac{dV_G}{dT}\right)_m = \frac{\partial V_G}{\partial T} + \left(\frac{\partial V_G}{\partial pH}\right)\left(\frac{dpH}{dT}\right) \qquad (2\text{-}25)$$

According to equation (2-21), the temperature sensitivity varies with drain current I_D. Experimental results of $(\frac{dV_G}{dT})_m$ are given in Figure 2-10. The figure show us that a linear relationship exists between $(\frac{dV_G}{dT})_m$ and I_D, and a point where V_G is independent of the temperature can be found, when the devices are operated in the unsaturated region [14].

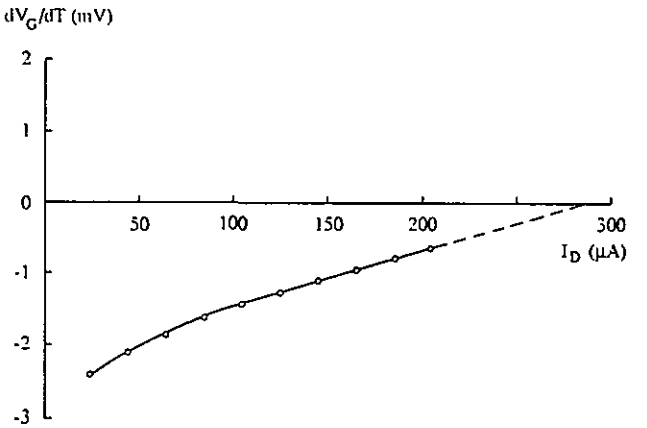

Figure 2-10. *Temperature sensitivity as a function of the drain current I_D. (V_D = 1.0 V, HCl-Tris buffer solution pH = 7.6, temperature range 15-30 ℃)*

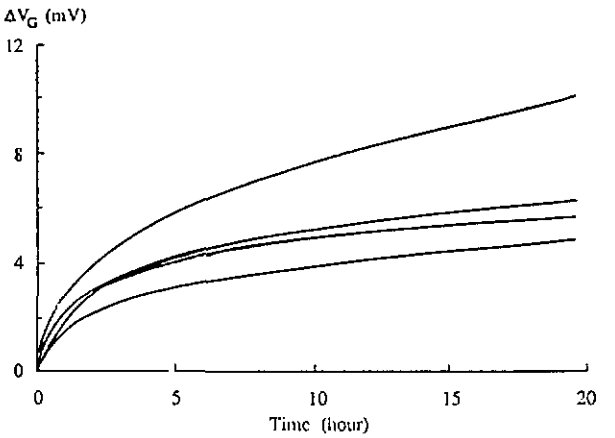

Figure 2-11. *Drift behavior of an ISFET at 25 ℃ in a HCl-Tris buffer solution. (V_D = 0.5 V, I_D = 100 μA).*

Drift behavior

The drift was measured during first exposure of the device into the HCl-Tris buffer solution as well as during subsequent exposures. Between exposures the devices were stored in a dry room at ambient temperature for one week. The results are shown in Figure 2-11 [15].

The drift during the first exposure is much higher than the subsequent exposures. In addition the drift during subsequent exposures is quite reproducible. After a stabilizing time of 10 hours, the drift value is less than 0.2 mV/hr.

The results for the first order terms of the Taylor series, have the linear behaviors under certain limited conditions, thus the second order terms of $\frac{\partial^2 V_G}{\partial pH^2}$, $\frac{\partial^2 V_G}{\partial T^2}$ and $\frac{\partial^2 V_G}{\partial t^2}$ at these conditions can be set equal to zero. The second order terms in function of pH and temperature, and of drift and temperature, as well as the correspondence with experimental results will be discussed in detail in chapter 5.

2.7 Conclusions

The experimental results can be summarized as the pH sensitivity has a value of about 55 mV at 25 °C in a pH region from pH 2 to pH 10 with a reproducibility of 0.5 mV/pH and a drift behavior less than 0.2 mV per hour. With such ISFETs the miniaturization of chemical sensors can be realized. However the problem of the stabilization still effects the applications of the ISFET because of the drift behavior. This problem and some solutions will be discused and proposed in chapters 5 and 6.

2.8 references

[1]. P. Bergveld, IEEE Trans. Biomed. Eng. Vol. BME-17, 1970, 70-71.

[2]. S. Caras and J. Janata, Anal. Chem., Vol. 52, 1980, 1935

[3]. M.J. Eddowes, D.G. Pedley and B.C. Webb, Sensors and Actuators, Vol. 7, 1985, 233.

[4]. H. Abe, M. Esasi and T. Matsuo, IEEE Trans. Electron Devices, ED-26, 1979, 1939-1944.

[5]. T. Akiyama, Y. Ujihara, Y. Okabe, T. Sugano and E. Niki, IEEE Trans. Electron Devices, ED-29, 1982, 1936.

[6]. M. Esahi and T. Matsuo, IEEE Trans. Biomed. Eng., BME-25, 1978, 184.

[7]. S.M. Sze, Physics of Semiconductor Devices, Wiley, New York, 1981.

[8]. J. Janata and R.J. Huber, In H. Freiser (Ed.) Ion-selective electrode in analytical chemistry, Vol. 2, Plenum Press, 1980, 107.

[9]. L. Bousse, N.F. de Rooij and P. Bergveld, IEEE Trans. Electron Device, Vol. ED-30, No. 10, 1983, 1263-1270.

[10]. T.W. Healy and L.R. White, Advan. Colloid Interface Sci., Vol. 9, 1978, 303-345.

[11]. L. Leistiko, Physica Scripta, Vol. 18, 1978, 445-450.

[12]. L. Vadasz and A.S. Grove, IEEE Trans. Electron Devices, Vol. ED-13, 1966, 863-866.

[13]. H.H. van den Vlekkert, N.F. de Rooij, Analysis, Vol. 16, No. 2, 1988, 110-119.

[14]. H.H. van den Vlekkert, Thesis, University of Neuchâtel, Switzerland, 1988.

[15]. C. Arnoux, Thesis, University of Neuchâtel, Switzerland, 1988.

CHAPTER 3
A pH-ISFET and a Combined pH-ISFET/ Temperature Sensor with Back-Side Contacts

parts of the chapter were presented at:

MICONEX 88, The 3rd Multinational Instrumentation Conference, BEIJING, China, 1988, 106-112.
"A combined pH-ISFET/Temperature sensors with back-side contacts".
B.HU, H.v.d.VLEKKERT, S.JEANNERET, and N.F.de ROOIJ.

TRANSDUCERS '87, TOKYO, Japan, 1987, 726-729
"A pH-ISFET and an integrated pH-pressure sensor with back-side contacts".
H.H.van den VLEKKERT, B. KLOECK, D.PRONGUE, J. BERTHOUD, B. HU, N.F. de ROOIJ, E. GILLI, and Ph.de CROUSAZ.

published in:

Sensors and Actuators, Vol. 14, No. 2, 1988, 165-176.
"A pH-ISFET and an integrated pH-pressure sensor with back-side contacts".
H.H.van den VLEKKERT, B. KLOECK, D.PRONGUE, J. BERTHOUD, B. HU, N.F. de ROOIJ, E. GILLI, and Ph.de CROUSAZ.

CHAPTER 3 A pH-ISFET and a Combined pH-ISFET/Temperature Sensor with Back-Side Contacts

3.1 Abstract

The pH-ISFET and the combined pH-temperature sensor with back-side contacts which are presented, consist of an insulated-gate field effect transistor for pH measurement and a diode for temperature measurement. In order to make a probe which has a diameter as small as possible after bonding and encapsulation, the contacts are fabricated on the back side of the chip. Electrical connection wires can be connected directly onto these contacts.

The final chip size is 1.5 mm * 1.5 mm. Al_2O_3 is used as the pH-sensitive layer. The top side of the sensor contains the ISFET and the temperature sensitive diode is located on the back side, sharing one contact with the source and substrate of the pH-ISFET.

3.2 Introduction

During the past years many articles appeared on the applications of ion-selective field effect transistors (ISFET) especially in the biomedical field [1]. It is imperative that the sensors are designed in regard to the required application and of the measurement conditions. One of the major problems which has prevented, until now, a wide application of these chemical sensors is their unreliable encapsulation.

Furthermore, if standard bonding and encapsulation techniques are used, the distance between the bond paths and the sensitive area that is exposed to the solution, has to be large enough in order to enable an adequate encapsulation. This requirement leads to increased sensor dimensions undesirable.

A solution for both problems is to locate the contacts on the back side of the sensor. To achieve this feed-through contacts through the silicon wafer must be fabricated. Several techniques to fabricate the feed-throughs in silicon have been reported: laser drilling [2], spark erosion [3], plasma etching [4,5], and other techniques such as ion beam milling [6], centrifugal etching [7], and diffused Al columns [8]. All these techniques need expensive equipment and/or high technical skills. The easiest and simplest technique to realize the contact from the back is to etch holes in the silicon substrate with an anisotropic etchant like potassium hydroxide [9] followed by a diffusion step.

Another problem is the temperature dependence of pH measurements. Since the pH value of the solution and the pH sensor are both temperature sensitive, the temperature should be known in order to give the correct pH value of the solution under investigation. For this reason a temperature sensor has to be integrated on the same chip. An example of such an approach has been published for a humidity sensor, based on FET technology where a temperature sensitive diode was integrated [11]. A new pH-temperature sensor is proposed here, based on the back side contacted ISFET [10] and on a temperature sensitive diode.

3.3 The Back-Side Contacts

The conventional contacts for bonding wires on MOSFETs (Metal Oxide Semiconductor Field Effect Transistor) and ISFETs are fabricated on the same side of the active surface and the wires are bonded by a bonding machine from the chip to a support. The ISFETs with the back-side contacts have contacts opposite to the active surface and the electrical wires are directly bonded in the contact holes on the back side. The chips with wires can be encapsulated when a smooth surface and a small size of sensor are required.

The back-side contacts consist of two parts: contact holes and inner electric connections. The holes are etched in the p-type substrate. The etching is anisotropic: in the <100> direction the etch rate is high, and in the <111> direction it is very low. Therefore the V-holes are formed in the <100> oriented wafer [9]. The etching is stopped when a membrane of 10 μm thick is left on the bottom of the holes. Alternatively the silicon is etched through, onto the SiO_2 protection layer on the top side. The dimension (l) of the hole bottom depends on the hole depth (d) and on the mask dimension (L) according to:

$$l = L - \frac{2d}{\tan(\alpha)} \qquad (3\text{-}1)$$

where $\alpha = 54.74°$ is the angle between the [100] and [111] planes.

For making the inner electric connections from one side of the wafer to another two different methods were studied. For one of these methods, the connections were formed by deep diffusion profiles in the silicon membranes and around the holes. The n-type diffusion was performed after etching the holes and a junction of 9 μm depth was obtained. Then the fabrication steps for making the ISFETs part on the top side were performed. The source and drain were formed over the membranes of the holes. They were connected to the n-type inner connections in the membranes after diffusion in these

steps. Aluminum deposited in the holes makes ohmic contacts. The fabrication process will be explained in detail in the next section. A cross section of the back-side contacts is shown in figure 3-1.

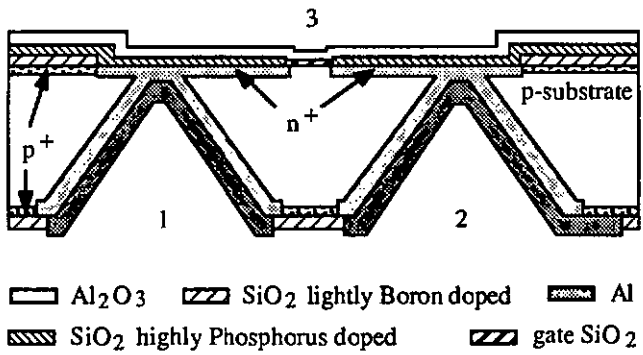

Figure 3-1. *Connections from the back-side contact holes to drain and source of the ISFET on the top-side were formed by the doped silicon membranes on the bottom of the holes. (1) drain, (2) source and (3) gate.*

For the second method the inner connections were formed by aluminum wires. These wires were made by metallizations from both sides. On the back side the contacts holes etched through silicon wafer, until a protection layer of SiO_2 on the top side of the wafer were reached. Then a SiO_2 layer was grown in the holes in order to insulate the aluminum contacts from the silicon substrate. After this step the aluminum contacts in the holes were formed by a metallization on the back side. An aluminum layer was obtained under the SiO_2 membranes on the top side. After metallization small holes were etched from the top side through the SiO_2 membranes to the aluminum layer. Then an aluminum layer was deposited on the top side. This layer connected to the contacts on the back side through the small holes. At the same time the connections between contacts to source and substrate, and to the drain were formed. A high temperature anneal made a good ohmic contact between the two Al layers on both sides in the last step. Figure 3-2 shows the cross section of the ISFET chip.

The top side of the ISFETs with back-side contacts fabricated with these two methods are shown in Figure 3-3. We compared these two methods during fabrication and found that the connections made by the Al wires had the following problems: the

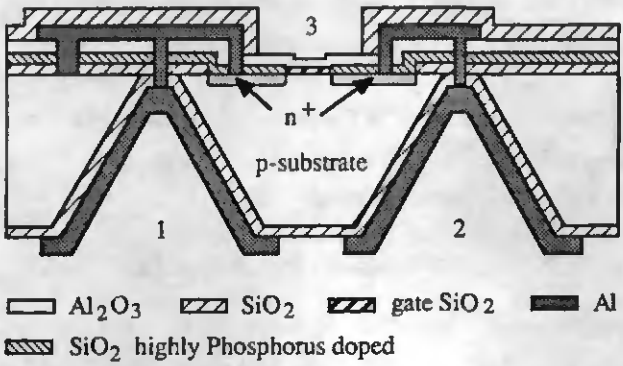

Figure 3-2. *Connections from back-side contacts holes to source and drain were formed by aluminium layers deposited from both sides. (1) source, (2) drain and (3) gate.*

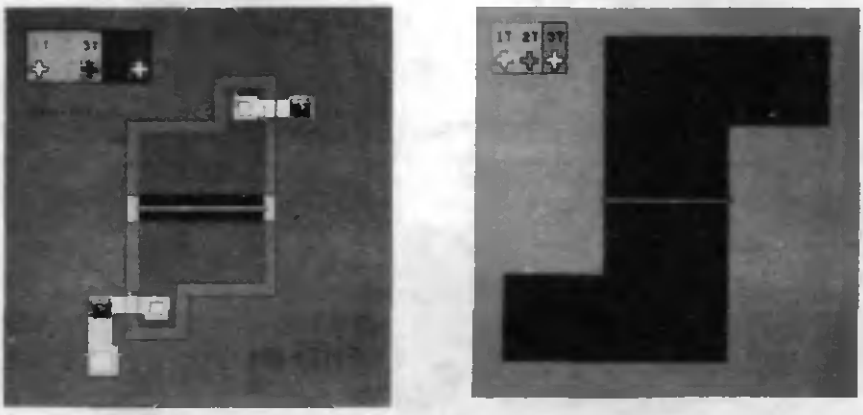

(a) (b)

Figure 3-3. *Top-side view of the chip with different inner connections. (a) the inter cross connections from back side contacts to drain and source on top side are formed by aluminium and (b) by diffusion through the silicon membrane under source and drain areas.*

process was more complicated and the SiO_2 membranes over the holes had a maximum thickness of 1 μm and they were very easy to break during the fabrication procedure. In order to simplify the fabrication process, only one of these fabrication methods of connections was chosen. The connection formed by the diffusion inner cross section was used in the further study. The connections made by Al wires had a contact resistance of 2.3 Ω. It could be usable for other applications.

3.4 Fabrication of the ISFET/Temperature Sensor with Back-Side Contacts

According to the requirement of the pH measurement, a temperature sensing diode was integrated on the ISFET chip also with back-side contacts. The sensors were fabricated on a p-type wafer having a thickness of about 280 μm and polished on both side. The contact holes were etched in a potassium hydroxide (KOH)/water solution from the back side, with a mask of silicon dioxide grown by wet oxidation on both sides. The

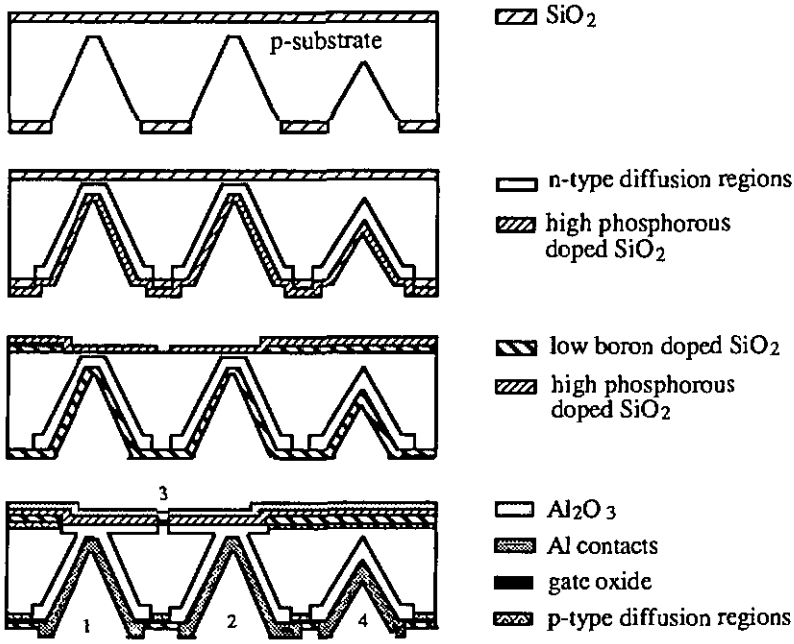

Figure 3-4. *Fabrication steps. 1) drain, 2) source and 3) gate of ISFET, 4) diode.*

holes had an area of 450 * 450 μm^2 at the surface and of about 55 * 55 μm^2 at the bottom. After opening larger windows around the contact holes for diffusion, the silicon dioxide doped with phosphorous was deposited on the back side by chemical vapor deposition (CVD), followed by a deep diffusion of about 9 μm depth through the thin membranes. Then all the oxide layers on both sides were etched away and silicon dioxide lightly doped with boron was deposited to form the channel stopper. After opening the windows for the source and drain on the top side, the phosphorous doped silicon dioxide was deposited. The oxide on the gate areas was etched to a size of 15 μm long and 500 μm wide. The gate oxidation and diffusion for the channel stopper, source and drain were done at the same time at 1100 °C. The gate is covered with 900 Å of SiO_2 with 600 Å Al_2O_3, deposited by CVD, over it. The last step consists of forming the aluminum contacts by a lift-off technique.

Simultaneously a temperature sensing diode is fabricated at the same time by using the same wire contact technique as for the ISFET. The substrate was used as the p-type region of the diode. The ISFET source, being connected to the p-type substrate, can serve as one contact of the diode. Hence only one supplementary hole is necessary, which is beneficial for the mechanical stability of the chip, as well as for the required chip surface. The contact hole for the diode was simultaneously etched with the contact holes for the ISFET, about 200 μm in depth and with an area of 300 * 300 μm^2. The n-type region of the diode was then formed by an n^+-type diffusion in the hole at the same time as the deep diffusion for the ISFET contacts. The chip was designed with minimal dimensions allowed by the size of the contact holes: 1.5 mm by 1.5 mm. The fabrication process is shown in figure 3-4. After dicing the wafer, electrical wires were directly glued into the three contact holes by means of a conductive epoxy. Finally the back side and side walls of the chip were encapsulated with epoxy. The ISFET/Temperature sensor chip with back-side contacts is shown in Figure 3-5.

After fabrication of the sensors, the basic characteristics of the ISFET, such as pH-sensitivity, drift behavior and temperature sensitivity, and the temperature sensitivity of the diode were measured. The ISFET was operated in the constant current mode, at a drain current (I_D) of 100 μA and a drain-source voltage (V_D) of 0.5 V, using a specially designed amplifier system, with the gate-(reference electrode)-source voltage (V_G) as the output parameter [14]. The temperature sensing diode was fed with a current of 100 μA. Since the pH-ISFET and the temperature sensor have to be operated simultaneously, the influence of the diode on the ISFET characteristics was tested also.

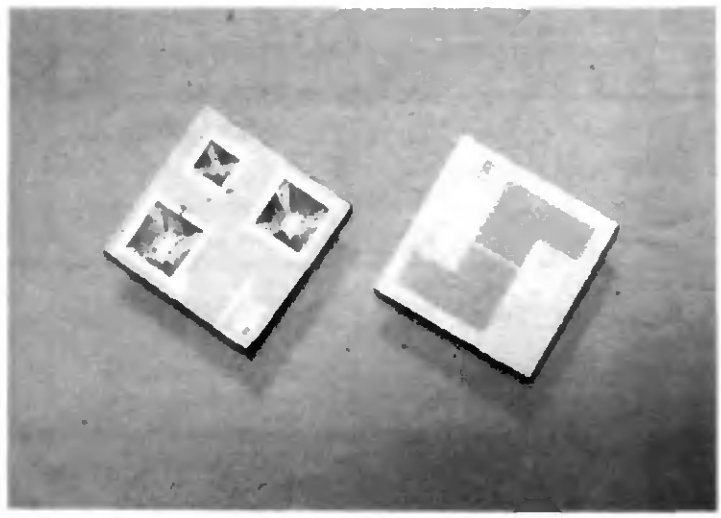

Figure 3-5. *Top side and the back side of the ISFET/Temperature sensor .*

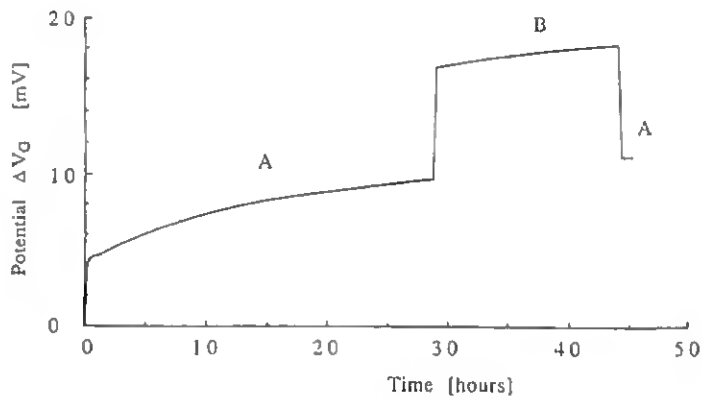

Figure 3-6. *Comparison of the drift measurement of the device with the diode (A) connected and (B) disconnected.*

3.5 Results and discussion

The pH sensitivity was tested by adding an acid or base to a HCl-Tris solution at 25 °C. The experimental result is about 55 mV/pH, with a reproducibility of 0.5 mV/pH between measurements.

The drift behavior was measured over 45 hours in a HCl-Tris solution (Tris 0.617 mol/l and HCl 0.5 mol/l, pH = 7.6) at 25°C. The sensors were measured several times with an interval of one week. Between measurements they were stored in dry ambient temperature. The diode was connected and disconnected during this measurement to investigate its influence. The drift when the diode was disconnected was less than 0.3 mV/h and quite reproducible between different measurements. Both results are comparable to other measurements with similar sensors [4,14,15]. When the diode was connected, an offset in the reference electrode to source voltage V_G was observed, but the pH-sensitivity and the drift for the ISFET remained the same, as illustrated in figure 3-6.

This offset in V_G can be explained as follows: the current through the diode also passes through the substrate, this can lead to a voltage drop, called V_{BS} (substrate bias).

V_G for an ISFET, operated in the linear region, is given by:

$$V_G = \frac{I_D L}{\mu_n W C_o V_D} + V_T + \frac{1}{2} V_D \qquad (3\text{-}2)$$

where μ_n denotes the electron mobility, W the channel width, L the channel length, C_o the insulator capacity and V_T the threshold voltage [16].

It is known that when a substrate bias is applied to a MOSFET, the threshold voltage changes accords to:

$$V_T = V_{FB} + 2\Psi_B + \frac{\sqrt{2\varepsilon_S q N_A (2\Psi_B + V_{BS})}}{C_o} \qquad (3\text{-}3)$$

where V_{FB} is the flat-band voltage, Ψ_B is the potential difference between the Fermi level and the intrinsic Fermi level, ε_S the permittivity, q the unit charge and N_A the acceptor impurities concentration [12].

The V_T for an ISFET is given by:

$$V_T = E_{ref} - \Psi_o + \chi - \frac{1}{q}\Phi_{Si} - \frac{Q_{ss}}{C_o} + 2\Psi_B + \frac{\sqrt{4\varepsilon_S q N_A \Psi_B}}{C_o} \qquad (3\text{-}4)$$

where E_{ref} denotes the reference electrode potential, Ψ_o the potential difference between the insulator surface and the bulk of the solution, χ the surface dipole potential at the

insulator/solution interface, $\frac{I}{q}\Phi_{Si}$ represents the silicon work function, Q_{ss} the insulator charge per unit area [13].

Since the substrate bias has the same effect on an ISFET as on a MOSFET, according to formula (3-3), expression (3-4) can be written as:

$$V_T = E_{ref} - \Psi_o + \chi - \frac{I}{q}\Phi_{Si} - \frac{Q_{ss}}{C_o} + 2\Psi_B + \frac{\sqrt{2\varepsilon_S q N_A (2\Psi_B + V_{BS})}}{C_o} \qquad (3\text{-}5)$$

Combined with (3-2), this confirms that V_G is a function of V_{BS}. As the pH sensitivity is determined by Ψ_o and the drift is caused by the alumina layer only [17], no influence on these parameters can be expected from the temperature diode. The temperature sensitivity of the ISFET, $(\frac{\partial V_G}{\partial T})$, however can change because of the temperature dependence of V_{BS}.

The temperature sensitivity is given by:

$$(\frac{\partial V_G}{\partial T}) = (\frac{\partial V_G}{\partial T})_{pH} + (\frac{\partial V_G}{\partial pH})_T (\frac{\partial pH}{\partial T}) \qquad (3\text{-}6)$$

The second term is caused by the temperature dependence of the pH of the solution [14]. In our case the temperature dependence of V_{BS} has to be taken into account too, resulting in:

$$(\frac{\partial V_G}{\partial T}) = (\frac{\partial V_G}{\partial T})_{pH,V_{BS}} + (\frac{\partial V_G}{\partial pH})_{T,V_{BS}} (\frac{\partial pH}{\partial T}) + (\frac{\partial V_G}{\partial V_{BS}})_{pH,T} (\frac{\partial V_{BS}}{\partial T}) \qquad (3\text{-}7)$$

The temperature sensitivity of the ISFET and the temperature sensitivity of the diode were tested by varying the temperature of the solution between 10 and 40 °C. The results of the temperature sensitivity test for two ISFETs are given in table 3-I. In the temperature range 10°C to 40°C, the difference of the temperature sensitivities that were measured on these ISFETs, $(\frac{\partial V_G}{\partial V_{BS}})(\frac{\partial V_{BS}}{\partial T})$, with the diode connected and disconnected is about -0.04 mV/°C, as demonstrated in Figure 3-7.

Figure 3-8 shows the output curve of the temperature sensor. The temperature sensitivity is 2.25 mV/°C which is comparable to a similar temperature sensitive diode [10].

Since the temperature diode slightly influences the temperature sensitivity of the pH-ISFET, another design for the temperature sensor which eliminates this influence was fabricated. it is presented in the next section.

Table 1. *Temperature sensitivities of the pH-ISFETs*

	Sensor No.2		Sensor No. 4	
T°C	V_G^* (mV)	V_G (mV)	V_G^* (mV)	V_G (mV)
10.3	403.16	396.71	531.27	530.38
15.1	398.97	392.35	527.48	526.9
19.9	394.13	387.22	523.33	522.59
24.6	389.82	382.67	519.84	518.95
29.7	385.07	377.65	515.77	514.82
34.6	380.77	373.21	512.41	511.21
39.2	376.96	369.96	509.31	508.01
$\frac{\partial VG}{\partial T}$ (mV/°C)	- 0.91	- 0.94	- 0.76	- 0.78

* Temperature sensing diode connected.

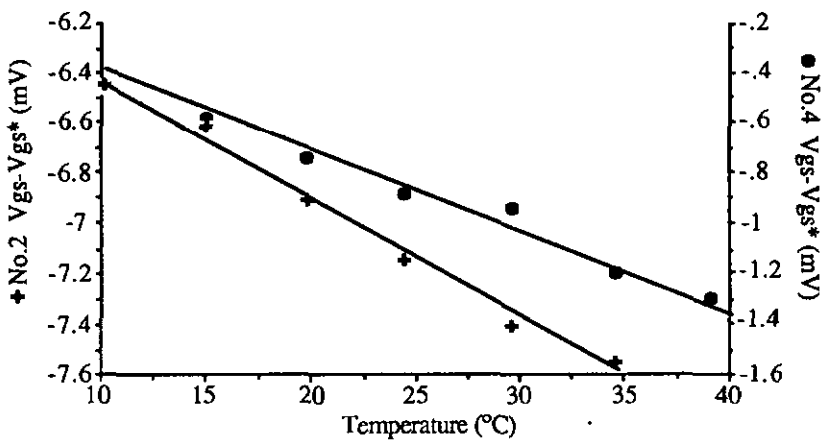

Figure 3-7. *The difference in V_G as a function of temperature for two ISFETs with the diode connected (V_G^*) and the diode disconnected (V_G).*

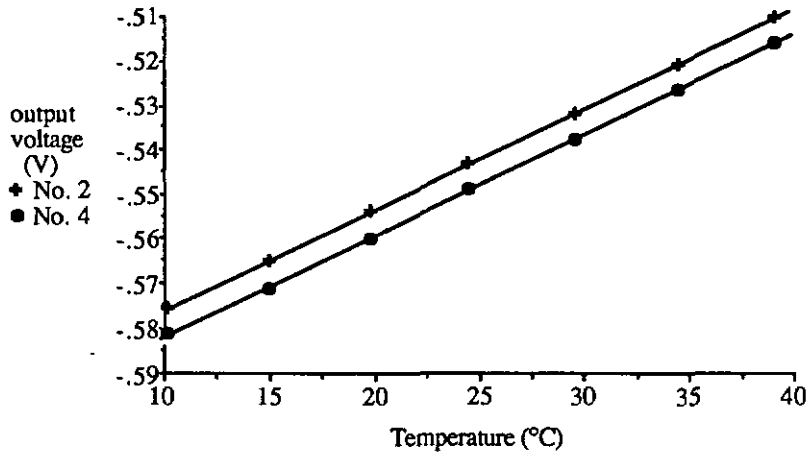

Figure 3-8. *Temperature measurements of the diodes of sensor No.2 and No.4. The sensitivity is 2.2 mV/°C for both.*

3.6 New design of the ISFET/Temperature sensor

In the new design the device had three back-side contacts also. The temperature sensitive diode shared a contact with the ISFET. In order to avoid the substrate bias another junction was made between p-type substrate and the diode. This was formed by a p-n-p structure. The n-type region of the diode was connected to the substrate. The current which passes through the diode is now isolated from the substrate by a junction formed with p-type substrate and n-type region.

The fabrication process of the new design needed two masks more than the old one: the first one for opening window for n-well and the second one for the p-type region of the diode. After deposition of the silicon oxide with high phosphorous doping for the contacts of the ISFET on the back side, the n-well region was opened with the first new mask and a lightly phosphorous doped SiO_2 layer was deposited. Then the deep diffusion for the contacts and n-well was performed. The window for the p-type region was opened on the contact hole of the diode after deposition of the phosphorous doped SiO_2 for the source and drain area. Then a CVD SiO_2 layer, doped with boron, was deposited on the back side. The p-type region of the diode was formed during the gate oxidation and the diffusion for source and drain. The fabrication steps are shown in figure 3-9.

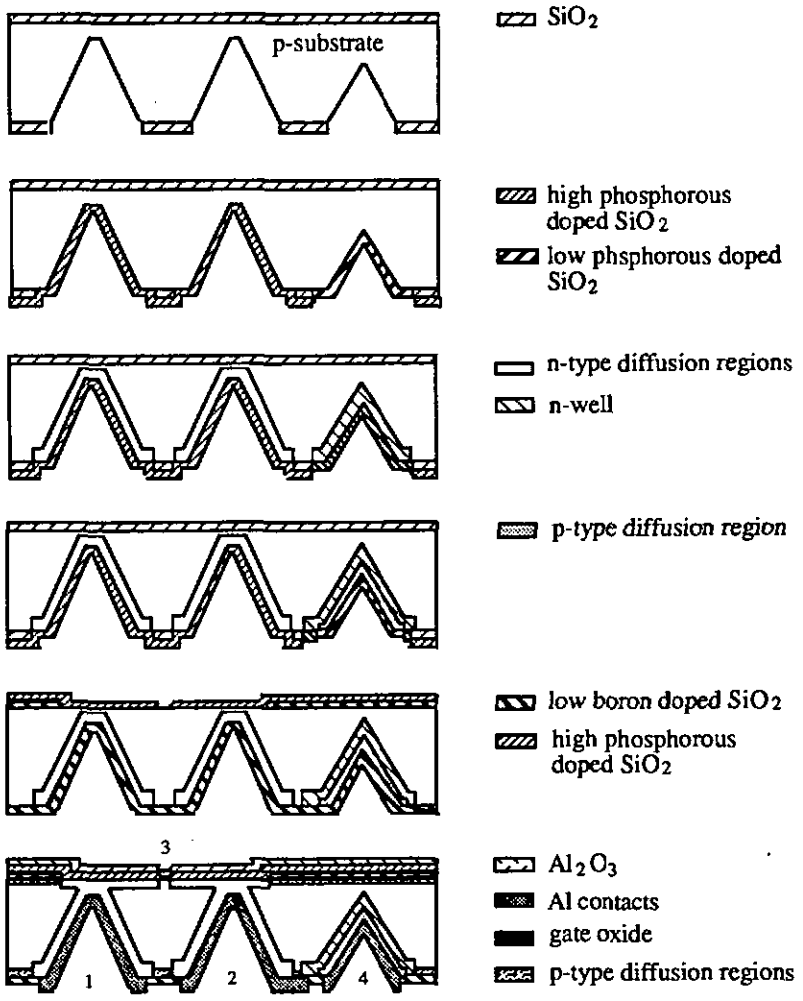

Figure 3-9 *Fabrication steps of the new design. 1) drain, 2) source and 3) gate of ISFET, 4) diode.*

The characteristics of the sensor of the new design were then tested. It showed a similar pH sensitivity, temperature response and drift behavior as those of a normal ISFET [17,18]. The offset of V_G with the diode connected or disconnected during drift measurement is zero. Figure 3-10 shows the results of the drift measurement.

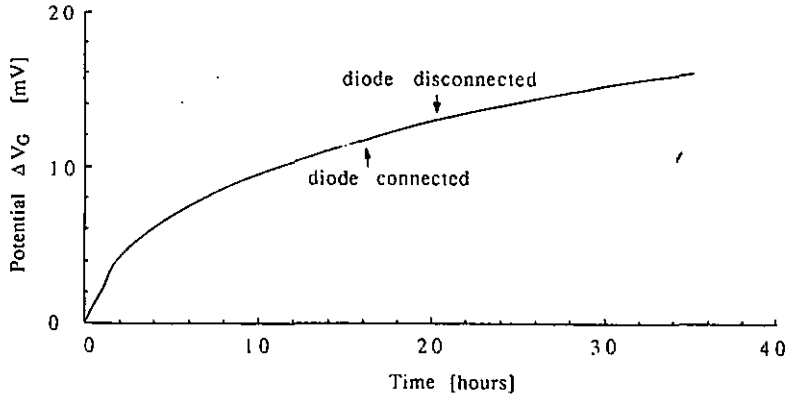

Figure 3-10. *Comparison of the drift measurement of the new device with the diode (a) connected and (b) disconnected.*

3.7 Conclusions

We have shown the possibility to realize an ISFET and an integrated pH-temperature sensor with small dimensions. The pH characteristics are comparable to standard pH sensitive ISFETs with alumina as the pH sensitive layer [14,15,17]. Using this contact technique the sensors are used for example in measurements of interdental plaque pH, where the sensor should be at the same level as the human enamel piece into which it is mounted as illustrated in Figure 3-9. Another application is an integrated pH-pressure sensor for in-vivo measurements where the normal ISFET can not be used [19]. A third important application in gas sensors will be presented in the next chapter.

In this study we found that when a current past through the substrate the temperature sensitivity of the ISFET was changed with a diode integrated on the same chip without isolation to the substrate, but the pH-sensitivity and the drift for the ISFET remained the same. We can imagine that the temperature sensitivity of the ISFET should be changed with the different current. Therefore this current could be used as a temperature compensation of the ISFET.

Figure 3-11 A back-side contacted pH-ISFET mounted in a partial denture.

3.8 References

[1]. J. Koryta, Anal. Chim. Acta, Vol. 183, 1986, 1-46.

[2]. D.J. Ehrlich, D.J. Silversmith, R.W. Mountain, and J. Tsao, IEEE Trans. Components, Hybrids, Manuf. Technol., Vol. CHMT-5, No. 4, 1982, 520-521.

[3]. C. van Osenbrugge, Philip Tech. Rev., Vol. 30, 1969, 195.

[4]. C. Tung, Master thesis, Case Western Reserve Univ., Cleveland, OH, 1984.

[5]. M. Ameen, M. Monfils, Z. Hasan, and D. Gates, Semiconductor International, Sept. 1988, 122-128.

[6]. D. Bollinger and R. Fink, Solid State Technol., Vol. 25, 1980, 79-84.

[7]. H. Kuiken and R. Trjburg, J. Electrochem. Soc., Vol. 130, No. 8, 1983, 1722.

[8]. T. Anthony and H. Cline, J. Appl. Phys., Vol. 49, 1978, 2777.

[9]. K. E. Bean, IEEE Trans. Electron Devices, Vol. ED-25, No. 10, 1978, 1185.

[10]. H. H. van den Vlekkert, B. Kloeck, D. Prongue, J. Berthoud, B. Hu, N. F. de Rooij, E. Gilli, and Ph. de Crousaz, Transducers '87 the 4th International Conference on Solid-State Sensors and Actuators (Tokyo), 1987, 726-729.

[11]. M. Hijikigawa, T. Sugihara, J. Tanaka, and M. Watanabe, IEEE Transducers '85 International Conference on Solid-State Sensors and Actuators, 1985, 221-224.

[12]. S. M . Sze, Physics of Semiconductor Device, 2nd edition, 1981, 431.

[13]. L. Bousse, N. F. de Rooij, and P. Bergveld, IEEE Trans. Electron Devices, ED-30, 1983, 1263.

[14]. C. Arnoux, B. Kloeck, H. v. d. Vlekkert, and N. F. de Rooij, Proc. SSC-ASMT, 1985, 37.

[15]. H. Abe, M. Esashi, and T. Matsuo, IEEE Tran. Electron Devices, ED-26 No. 12, 1979, 1939-1944.

[16]. J. Janata and R. H. Huber, In H. Freiser (Ed.) Ion-selective electrodes in analytical chemistry, vol. 2, Plenum Press, 1980, 107.

[17]. H.H.van den Vlekkert and N.F.de Rooij, Analusis, Vol. 16,.No. 2, 1988, 110-119.

[18]. Chapter 2 of this thesis.

[19]. H.H.van den Vlekkert, B. Kloeck, D. Prongue, J. Berthoud, B. Hu, N.F. de Rooij, E. Gilli, and Ph. de Crousaz, Sensors and Actuators, Vol. 14, No. 2, 1988, 165-176.

CHAPTER 4
Application of the ISFET/Temperature sensor for the Carbon dioxide electrode

part of the chapter was presented at:

EUROSENSORS II, 4th symposium on sensors and actuators, 1988, ENSCHEDE, the Netherlands. "**Carbon Dioxide Gas Sensing Electrode Based on a pH-ISFET with Back-side Contacts**". B.Hu, H. H. van den Vlekkert. and N.F.de Rooij.

published in:

SENSORS AND ACTUATORS, Vol. 17, No. 1/2, 1989, "**Carbon Dioxide Gas Sensing Electrode Based on a pH-ISFET with Back-side Contacts**". B.Hu, H. H. van den Vlekkert. and N.F.de Rooij.

patent applications:

Switzerland patent application, No. 0406/88-8, 1 Jan 1988, "**Capteur de mesure de la concentration d'un gaz dans un fluide**"
Nicolaas de Rooj, Hans van den Vlekkert and Bo Hu.

France patent application, No. 88 14831, 15 Jan 1988, "**Capteur de mesure de la concentration d'un gaz dans un fluide**"
Nicolaas de Rooj, Hans van den Vlekkert and Bo Hu.

U.S.A. patent application, No. "**SENSOR MEASURING THE CONCENTRATION OF A GAS IN A FLUID**"
Nicolaas de Rooj, Hans van den Vlekkert and Bo Hu.

CHAPTER 4 Application of the ISFET/Temperature sensor for the Carbon dioxide electrode

4.1 Abstract

A novel carbon dioxide sensing electrode based on the Severinghaus principle has been developed. A pH-ISFET with back-side contacts is used as the internal pH sensing element and a temperature sensitive diode is integrated on the same chip. The sensor uses a Ag/AgCl wire as a reference electrode.

4.2 Introduction

Normally a pH glass electrode is used as the internal pH sensing element for a carbon dioxide electrode based on the Severinghaus principle [1] which is already widely used in the chemical analyzing system and in biomedicine [2,3,4]. However when a miniaturized electrode is required this pH glass electrode poses some problems: an increasing impedance and increasing response time with decreasing size. In order to solve these problems the pH-ISFET can be used instead of the pH glass electrode [5,6]. Another important factor which influences the response time of a carbon dioxide electrode, apart from the gas permeable membrane, is the gap between this membrane and the pH sensor. Using a normal ISFET having the active surface on the same side as the contacts, the encapsulation makes it difficult to achieve a minimum distance gap that is sufficiently. In order to decrease this distance as much as possible a pH-ISFET with back-side contacts was used [7].

To improve the performance of the carbon dioxide sensor further, the temperature sensitivity of the device has to be compensated [8]. Therefore a temperature sensor (diode) was integrated on the ISFET chip.

4.3 Theory

In the classical Severinghaus electrode configuration a gas permeable membrane is placed between the sample solution and the measuring cell which consists of a pH sensitive glass electrode, a reference electrode and an intermediate electrolyte layer (see figure 4-1). The carbon dioxide diffuses through the gas permeable membrane until the following equilibrium is established between the inner electrolyte solution and the external sample:

$$CO_2 \text{ (sample)} <=> CO_2 \text{ (membrane)} <=> CO_2 \text{ (inner electrolyte film)}$$

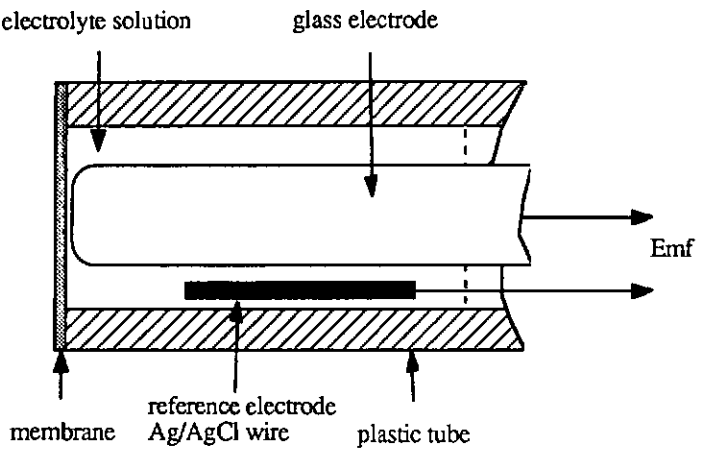

Figure 4-1. *Diagram of the CO_2 sensor using a glass electrode as a pH sensing element.*

In this equilibrium state the response of the electrode changes according to the pH of the inner electrolyte solution which is governed by the following equilibria when the pH < 8 [9]:

$$CO_2 + H_2O <=> H_2CO_3 \qquad K_h = \frac{[H_2CO_3]}{[CO_2]} \tag{4-1}$$

$$H_2CO_3 <=> H^+ + HCO_3^- \qquad K_a = \frac{[H^+][HCO_3^-]}{[H_2CO_3]} \tag{4-2}$$

For subsequent calculations it is more convenient to work with the total analytical concentration of carbon dioxide, $[CO_2] + [H_2CO_3]$, where the resulting K_1 value is the product of K_h and K_a from equations (4-1) and (4-2). It is expressed in equation (4-3).

$$K_1 = \frac{[H+][HCO_3^-]}{[CO_2]+[H_2CO_3]} = 4.45 * 10^{-7} \tag{4-3}$$

It must be noted that these equations describe the situation only when the pH of the internal electrolyte layer is lower than pH 8. If the pH > 8, other reactions can occur, such as: $CO_2 + OH^- <=> HCO_3^-$.

The relationship between the pH of the inner electrolyte solution and the concentration of the inner electrolyte CO_2 film is given by the Henderson-Hasselbalch buffer equation:

$$pH = pK_1 - \log(\frac{[CO_2]}{[HCO_3^-]}) \qquad (4\text{-}4)$$

In the equation, when the concentration of the $NaHCO_3$ is moderately (10^{-3} - 10^{-2} mol/l) high and at constant ionic strength the hydrogen carbonate ion activity can be considered constant. The surface potential is only a function of the $\log(P_{CO_2})$. At this range of the $NaHCO_3$ concentration, the sensitivity (S) of the electrode is presented as [1]:

$$S = \frac{\partial pH}{\partial \log(P_{CO_2})} = -1 \qquad (4\text{-}5)$$

where pH is the pH of the internal electrolyte solution and P_{CO_2} the partial pressure of CO_2.

The electrode using the pH-ISFET instead of the glass electrode functions on the same chemical mechanism hence the same sensitivity S as that given by equation (4-5) acts on the sensor. The pH value of the internal electrolyte solution is measured by the pH-ISFET. The pH sensitive mechanism of the pH-ISFET is based on the surface reaction which gives rise to the surface potential Ψ_o as given by [10]:

$$\Psi_o = \frac{\beta}{\beta+1}\frac{2.303kT}{q}(pH_{pzc}-pH) \qquad (4\text{-}6)$$

where pH_{pzc} is the pH at the point of zero charge, ß is a dimensionless pH sensitivity parameter, q is unit charge, k is the Boltzmann constant and T is the absolute temperature. The voltage response to the CO_2 concentration is obtained by combining equations (4-6) and (4-5):

$$\Psi_o = \frac{\beta}{\beta+1}\frac{2.303kT}{q}(pH_{pzc} + \log(P_{CO_2})) \qquad (4\text{-}7)$$

Therefore based on the Severinghaus principle and the function of the ISFET, the characteristics of the CO_2 sensor can be derived in CO_2 sensitivity, drift behavior and time response and temperature sensitivity.

<u>CO_2 sensitivity</u>

According to the equations (4-7) and (4-5), the CO_2 sensitivity of the sensor is derived as:

$$\left(\frac{\partial V_G}{\partial \log(P_{CO_2})}\right)_{T,I} = -\left(\frac{\partial \Psi_o}{\partial \log(P_{CO_2})}\right)_{T,I} = -2.303\,\frac{kT}{q}\,\frac{\beta}{\beta+1} \qquad (4\text{-}8)$$

The sensor has the same sensitivity for $\log(PCO_2)$ as the pH-ISFET for pH with the opposite sign.

Drift behavior and time response

When the chemical equilibrium is considered stable, the drift behavior of the sensor is dependent on the ISFET and reference electrode which is caused by the aging of the Ag/AgCl wire in the electrolyte solution. Since the drift of the reference electrode is very small, the corresponding drift behavior of the CO_2 sensor is similar to the drift of the ISFET at equilibrium.

Another time characteristic which is important for the CO_2 sensor is the response time. It depends on several parameters such as the membrane material and the membrane thickness, the thickness of the electrolyte film at the pH electrode i.e. the gap, and the concentrations of CO_2 and of the HCO_3^- in the inner electrolyte.

In a theoretical treatment by Ross et al. [11] it is considered that the transport of a gas across the gas permeable membrane to achieve an equilibrium partial pressure of the gas on each side of the membrane, is the rate limiting step. The equilibrium of the CO_2 concentrations on both sides of the membrane are illustrated in Figure 4-2.

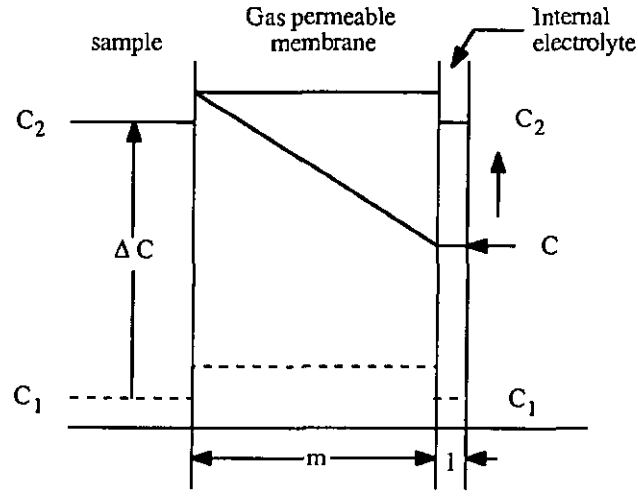

Figure 4-2. *Steady state model for electrode response.*

The electrode response time can be described by the following equation:

$$t = (\frac{l \cdot m}{D \cdot k})(1 + \frac{dC_B}{dC}) \cdot \ln(\frac{\Delta C}{\varepsilon C_2}) \qquad (4\text{-}9)$$

where l denotes the electrolyte film thickness, m is the membrane thickness, D is the diffusion coefficient of the CO_2 through the membrane, k is the partition coefficient of CO_2 between the aqueous solution and the membrane material, C_2 is the final concentration of CO_2 in the sample solution. ΔC is the difference of the initial and final CO_2 concentrations in the sample solution, C_B is the sum of the concentrations of all the other forms (i.e. HCO_3^-,CO_3^{-2}) in the inner electrolyte film, C concentration of H_2CO_3 in the inner electrolyte film and ε is defined as the fractional approach to equilibrium calculated by:

$$\varepsilon = |\frac{(C_2 - C)}{C_2}| \qquad (4\text{-}10)$$

For analytical purposes it is generally most convenient to speak of $t_{0.01}$ as the time required to reach 99% of the equilibrium, where $\varepsilon = 0.01$. In practice $\frac{dC_B}{dC}$ is considered in two simple cases [11]:

(a) $\frac{dC_B}{dC} \ll 1$

(b) the range $C_2 - C_1$ is sufficiently small so that $\frac{dC_B}{dC}$ can be considered constant, where C_1 is the initial concentration of CO_2 in the sample solution.

From equation (4-12) we can find that the time response depends on the direction of the concentration change. Going from a low to high concentration the time response which is nearly independent of the magnitude of the concentration change is shorter than that of the reverse process where the time response varies with the ratio $\frac{C_1}{C_2}$. The model as described by equation (4-9) predicts the effects of geometry, (l·m); membrane characteristics, (D·k); electrolyte composition, $\frac{dC_B}{dC}$; experimental conditions, $\frac{\Delta C}{C_2}$, on the time response of the electrode.

Temperature sensitivity

The total temperature effect on the CO_2 sensor is composed of effects of the reference electrode, the chemical equilibrium, surface potential caused by interaction in the interface between the electrolyte solution and the sensitive layer, and the solid state part of the ISFET. If the effects of the solid state and interaction in the interface are only

taken into account, the temperature sensitivity is equal to the temperature sensitivity of the pH-ISFET. An important part of the temperature sensitivity is due to the Ag/AgCl wire reference electrode, in the inner electrolyte solution with a concentration of NaCl of 11 mmol/kg. It has a high temperature sensitivity. In this case the temperature sensitivity of the sensor is given by:

$$\left(\frac{\partial V_G}{\partial T}\right)_{\log(Pco_2),t} = \frac{\partial V_T^{MOST}}{\partial T} + \frac{\partial E_{ref}}{\partial T} - \frac{\partial \Psi_o}{\partial T} - \frac{I_D\ L\ b}{\mu_n^o\ W\ C_o\ T_o\ V_D} \qquad (4\text{-}11)$$

However the temperature coefficient of the chemical equilibrium which contains the change of CO_2 solubility, chemical equilibrium between the CO_2 and the electrolyte solution and effects on the permeable membrane [12] changes the surface potential, so that the $\frac{\partial V_G}{\partial T}$ of the CO_2 sensor is different from that of the individual ISFET.

4.4 Experimental

The basic structure of the device is illustrated in Figure 4-3. A pH-ISFET and a temperature sensitive diode are integrated on the same chip with back-side contacts. A detailed description of the fabrication process can be found elsewhere [7,13,15]. The dimensions of the final chip are 1.5 mm *1.5 mm.

Only three contact wires are needed (drain, source/substrate/diode and diode), which can be glued directly into the back-side contact holes. Two plastic tubes are now used for the final assembly. The first one, with the same internal diameter as the chip, contains in the tip, the chip encapsulated with epoxy, with its surface aligned to the end of the tube. A Ag/AgCl wire passes through the wall of this tube. Figure 4-4 shows a picture of the ISFET with reference electrode (Ag/AgCl wire) after encapsulations.

The second tube into which the small tube with the ISFET and Ag/AgCl wire can be placed with the internal electrolyte solution has a larger diameter. On top of this second tube, a gas permeable membrane is solvent cast. The membrane material is a block copolymer of dimethylsiloxane and bisphenol-A-carbonate (Petrarch Systems Inc.). The active surface of the ISFET is placed as close as possible to this membrane. Finally the device is filled up with the internal electrolyte solution. The CO_2 sensor is shown in Figure 4-3.

The ISFET was operated in the constant current mode, at a drain current (I_D) of 100 μA and a drain-source voltage (V_{DS}) of 0.5 V. The temperature sensitive diode was operated with a current of 100 μA.

The drift behavior of the ISFETs and Ag/AgCl reference electrode was measured in the inner electrolyte solution (S45216 Electrolyte solution, RADIOMETER) against a Ag/AgCl double junction reference electrode. The pH sensitivity of the ISFET was tested by adding acid or base to a HCl-tris solution. A glass electrode was used as reference system.

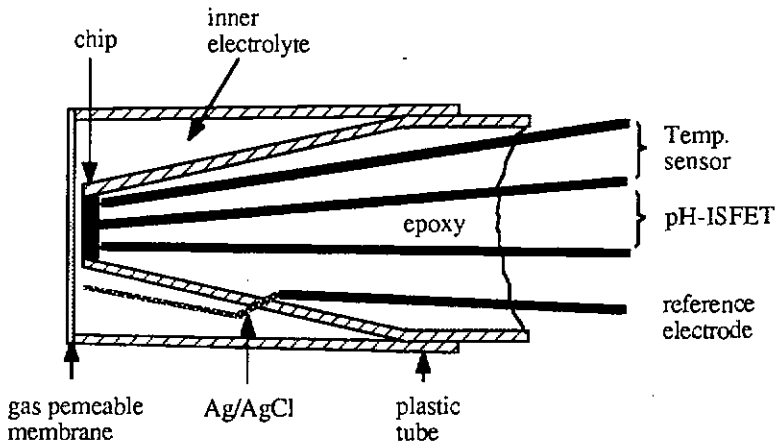

Figure 4-3. *The CO_2 sensor using a pH-ISFET as a sensing element.*

The CO_2 sensitivity S of the whole CO_2 sensor was measured using a pH 4 buffer solution through which gas mixtures with different concentrations of CO_2 (2%, 10% and 20%) were bubbled. By transferring the sensor to different concentrations the response time of the sensor was tested. The temperature sensitivity of the sensor was measured and the temperature response time of the sensor was determined using the temperature sensitive diode. The sensors were tested several times and stored dry at room temperature between measurements.

The temperature effect on the Ag/AgCl wire which was the reference electrode of the CO_2 sensor was tested in the inner electrolyte solution of the sensor with a temperature range from 10 °C to 35 °C. It was determined by using the potential measurements between Ag/AgCl wires and a glass electrode. In order to avoid the effect of the temperature on the glass electrode, two glass cells were used. The glass electrode was kept in one cell with the electrolyte solution at a constant temperature as well as constant pH and the Ag/AgCl wires was put in another measuring cell where the temperature was changed. In order to connect these two cells, a liquid bridge was made with a U glass tube filled up with electrolyte solution and the ends of the tube were blocked up with cotton plugs. When the ends of the tube were put in these cells, a liquid junction of the

Figure 4-4. *The encapsulated ISFET with a reference electrode (Ag/AgCl wire).*

Figure 4-5. *The completed CO_2 sensor .*

electrolyte solution from one cell to the other was formed. This measuring system is shown in Figure 4-6.

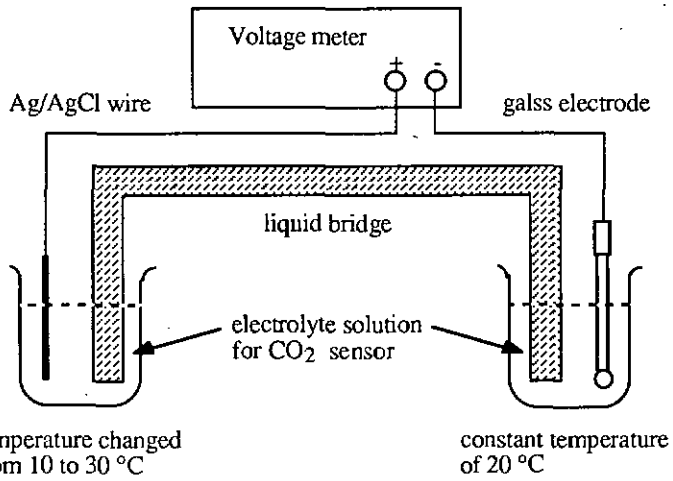

Figure 6. *Experimental set-up for the measurement of temperature effects of the Ag/AgCl wire electrode.*

4.5 Results and discussions

The Figure 4-7 shows the pH sensitivity of the ISFET and Pco_2 sensitivity (using the same ISFET as the pH sensing element) of the CO_2 sensor. They have a sensitivity of about 58 mV/pH for the ISFET and - 56 mV/decade for CO_2 measurement at 25 °C. These results are in agreement with equation (4-8), the sensitivity of the pH is equal to $\log(Pco_2)$.

The drift of the sensor is less than 0.23 mV/h (the pH-ISFET < 0.2 mV/h and the Ag/AgCl reference electrode < 0.03 mV/h) and reproducible.

A fast equilibrium response time is critical for a CO_2 electrode used for continuous measurement. Experimentally, response times of less than 1 min (90%) were obtained when going from 20% to 10% CO_2 with the membrane made of the block copolymer. The response of the CO_2 sensor upon fast changes of CO_2 is shown in figure 4-8.

The gap between the active surface of the ISFET and gas permeable membrane is about 100 µm and is dependent upon the handmade encapsulation of the chip. The response time of the sensor is quite fast and comparable with other types of CO_2 electrodes [5].

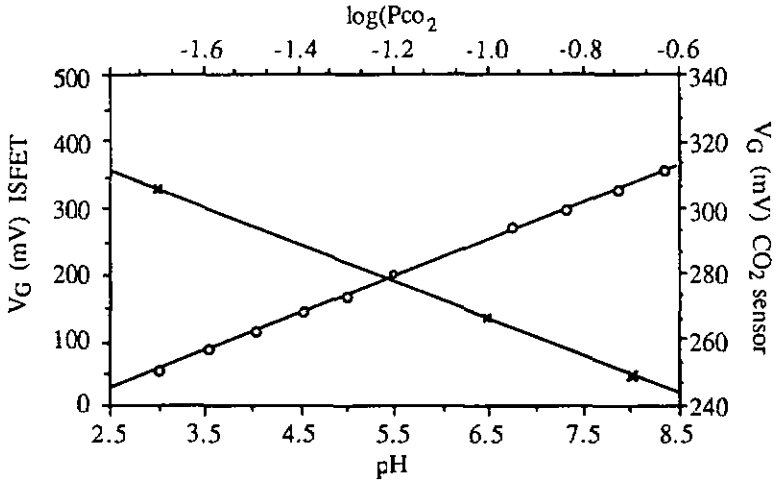

Figure 4-7. *The pH sensitivity of 58.2 mV/pH of the ISFET (o) and the pCO_2 sensitivity of -56.2 mV/log(P_{CO_2}) the CO_2 sensor (x) with some ISFET.*

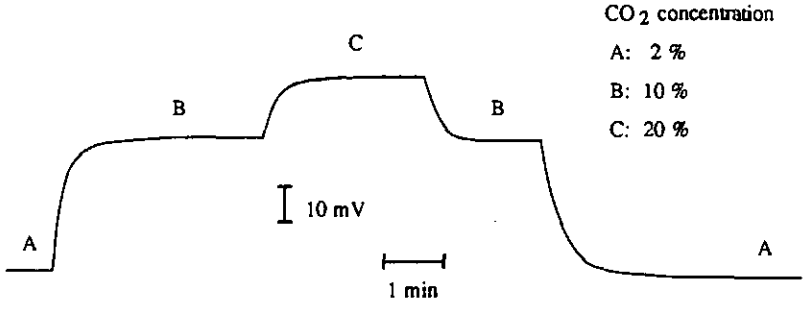

Figure 4-8 *Response time test of the CO_2 sensor.*

In practice, the CO_2 concentration in the cell changes with temperature due to the temperature dependence of the solubility of the CO_2 in the sample solution, chemical equilibrium and the effect on the membrane etc.. It results in changes of pH in the inner electrolyte solution. The measurements of the temperature sensitivity of the CO_2 sensor include all of these changes as well as the temperature coefficient of the pH-ISFET (the pH temperature dependence is not taken into account) and reference electrode (Ag/AgCl wire). Figure 4-9 shows the comparison of the temperature sensitivity of the pH-ISFET in HCl-tris buffer solution and the CO_2 sensor that was measured in the pH 4 buffer

solution through which gas mixtures with 10% CO_2 gas were bubbled. The same ISFET was used in these measurements.

From this figure, we seen that the temperature sensitivities of the CO_2 sensor and pH-ISFET are much different. This difference is independent on the solid state part of ISFET as the same ISFET was used.

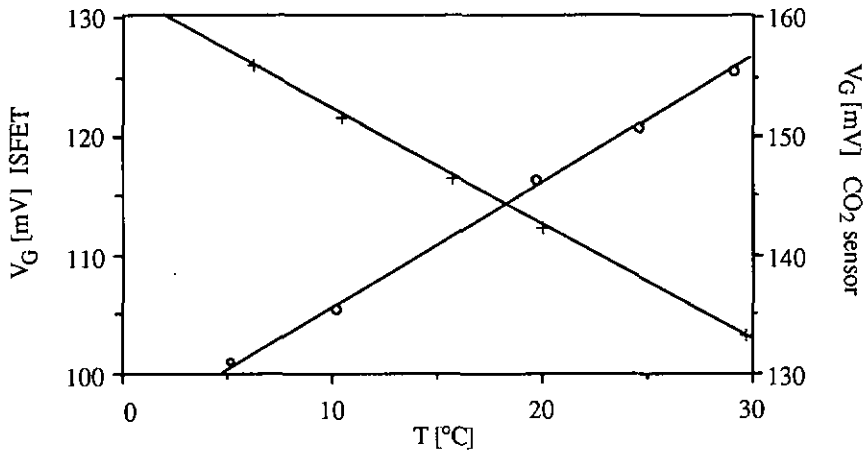

Figure 4-9. *Temperature sensitivity of -0.968 mV/°C for pH-ISFET (+) in the HCl-tris buffer and of 1.055 mV/°C for CO_2 sensor (o) in 10% CO_2 with the same ISFET os pH sensitive element.*

In the measurements of the temperature sensitivity at different pH or pCO_2, the result of minimal influence on the temperature sensitivity in large steps of changes of pH or CO_2 was obtained. Therefore we suppose that the pH value of the inner electrolyte solution, in the case that the 10% CO_2 sample is measured, is equal to the pH value of the HCl-tris buffer solution at 25 °C for ISFET, because the outputs of the ISFET in these solutions are similar.

According to the same measuring mechanism of the pH temperature sensitivity of the solution, the temperature sensitivity of this CO_2 sensor can be given by:

$$\left(\frac{\partial V_G}{\partial T}\right)_m = \left(\frac{\partial V_G}{\partial T}\right)_{pCO_2} + TCE + \frac{\partial E_{ref}}{\partial T} \qquad (4\text{-}12)$$

TCE is the temperature coefficient of the chemical equilibrium of the CO_2 sensor.

Considering the results obtained with the ISFET and the CO_2 sensor, the temperature coefficient of the chemical equilibrium (including effects on the solubility, chemical reaction and permeable membrane etc.) can be calculated. The measured and

calculated values of the temperature coefficients of each term for a CO_2 sensor and the ISFET in the temperature range between 5 °C and 30 °C are listed in Table 4-I.

Table 4-I The comparison of the temperature coefficient values for ISFET and CO_2 sensor.

pH-ISFET	HCl-tris	CO_2 sensor	10% CO_2 in pH 4
$(\frac{\partial V_G}{\partial T})_{sum}$	- 0.968 mV/°C [1]	$(\frac{\partial VG}{\partial T})_{sum}$	1.054 mV/°C [1]
$\frac{\partial V_G}{\partial pH}$	58.2 mV/pH [1]	$\frac{\partial V_G}{\partial pCO_2}$	- 56.2 mV/pH [1]
$\frac{\partial E_{ref}}{\partial T}$ (refe. elec.)	0.013 mV/°C [1]	$\frac{\partial E_{ref}}{\partial T}$ (Ag/AgCl)	0.623 mV/°C [1]
$\frac{\partial pH}{\partial T}$	- 0.027 pH/°C [1]	$(\frac{\partial V_G}{\partial T})_{pCO_2}$	0.589 mV/°C [2]
$\frac{\partial V_G}{\partial pH} * \frac{\partial pH}{\partial T}$	- 1.57 mV/°C [2]	TCE**	-0.158 mV/°C [2]
$(\frac{\partial V_G}{\partial T})_{pH}$	0.589 mV/°C [2]		
$\frac{\partial^2 V_G}{\partial T \partial I_D}$	0.01 mV/°CμA [1]	$\frac{\partial^2 V_G}{\partial T \partial I_D}$	0.01 mV/°CμA [1]

** the temperature coefficient of the chemical equilibrium of the CO_2 sensor.

1. the measured value.

2. the calculated value.

In this temperature range a temperature coefficient of 1.054 mV/°C on the CO_2 sensor potential at 10 % CO_2 in pH 4 buffer solution was obtained. When the temperature dependence of the pH-ISFET, which is independent to pCO_2, is removed, a temperature sensitivity of 0.465 mV/°C was calculated, this includes the temperature effect on the reference electrode. This result is comparable to that of the temperature effect on the potential of the pCO_2 electrode using the glass electrode as a pH sensitive element at 9.6 mol % CO_2 (factory premixed 10% gas mixture) in saline solution [12].

The temperature effect on the Ag/AgCl wires was found to be 0.623 ± 0.063 mV/°C. This result and subsequent error limits refer to one standard deviation of the statistical distribution of the measurements. Thus the temperature dependence of the chemical equilibrium could be calculated as given in the Table 4-1. Our evaluation does not allow an analysis of the individual contribution of each of the factors effecting the chemical equilibrium.

The change in the CO_2 sensitivity was 0.26 ± 0.1 mV/log(Pco2)°C, equal to the value given for similar pH-sensitive ISFETs [14].

In the Figure 4-10 the effect of fast temperature changes is shown. The sensor needs about three minutes to stabilize (temperature vs. time curve as measured with the temperature sensitive diode). The temperature off-set of V_G is also shown in this figure.

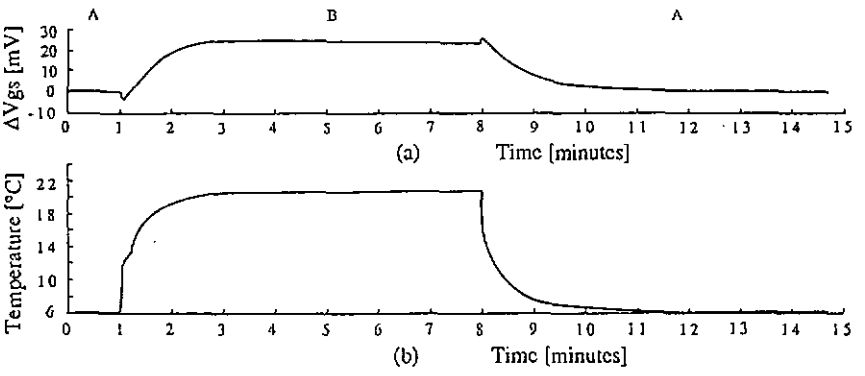

Figure 4-10 *(a) Temperature response time of the CO_2 sensor. A = 6 °C and B = 21 °C. (b) Temperature changes of the whole sensor measured by the diode.*

Comparing these two curves, it can be seen that the response time of the sensor to the changing temperature is very fast in that it follows the sensor's temperature curve, i.e. as the sensor's temperature increases the ΔV_G curve increase almost immediately. It indicates that the sensor has a very small heat capacity to be negligible between the sensitive surface of the ISFET and the sample solution.

4.6 Conclusions

The application of a pH-ISFET with back-side contacts as part of a CO_2 sensor has resulted in a sensor with good sensitivity. The very fast response time, to change in CO_2 concentration, and the small stabilization time, with respect to fast changes of temperature, result in a sensor which is capable of dealing with rapidly changing circumstances. The integration of the temperature sensitive diode enables the correction for the change in sensitivity upon change in temperature and can also be used for the correction of temperature off-set.

4.7 References

[1]. J. W. Severinghaus and A. F. Bradley, J. Appl. Physiol. 13 (1958), 515-520.

[2]. D. Midgley, Analyst, Vol. 100, 1975, 386-399.

[3]. E.E. Buzza, J.E. Leonard, H. Watanabe, and E.N. Carlsen, J. Association Advancement Medical Instrumentation, Vol. 4, No. 4, 1970, 136-144.

[4]. W.N. Opdycke, S.J. Parks, and M.E. Meyerhoff, Analytica Acta, Vol. 155, 1983, 11-20

[5]. K. Shimada, M. Yano, K. Shibatani, Y. Komoto, M. Esashi, and T. Matsuo, Med. Biol. Eng. Comput. Vol. 18, 1980, 741-745.

[6]. M. Nakamura, M. Yano, K. Shibatani, and K. Takakura, New Material & New Processes, Vol. 3, 1985, 367-371.

[7]. H. H. Van den Vlekkert, B. Kloeck, D.Prongue, J. Berthoud, B. Hu, N.F. de Rooij, E. Gilli, and Ph.de Crousaz, Proc.Transducers '87, Tokyo, Japan, June 1987, 726-730.

[8]. H. H. van den Vlekkert and N.F. de Rooij, Analusis, Vol. 16, No. 2, 1988, 110-119.

[9]. D.M. Kern, J. Chemical Education,Vol. 37, No. 1, 1960, 14-23.

[10]. L. Bousse, N.F. de Rooij, and P. Bergveld, IEEE Trans. Electron Device, Vol. ED-30, No. 10, 1983, 1263-1270.

[11]. J.W. Ross, J.H. Riseman, and J.A. Krueger, Pure Appl.Chem., Vol. 36, 1973, 473-487.

[12]. N.C. Lai, C.C. Liu, G. Brown, M.R. Neuman, and W.H. Ko, Medical and Biological Engineering, Vol. 13, No. 6, 1975, 876-882.

[13]. B.Hu, H. H. van den Vlekkert. S.Jeanneret, and N.F.de Rooij, Proc. Miconex '88, Beijing, China, May 1988 in press.

[14]. H.H.van den Vlekkert, L.Bousse, and N.F.de Rooij, J.Colloid and Interface Sci., Vol. 122, No. 2, 1988, 336-345.

[15]. Chapter 3 of this thesis.

CHAPTER 5
A novel Method of pH Measurement Based on Temperature Modulation on the ISFET

presented at:

The Third International Meeting on Chemical Sensors, CLEVELAND, U.S.A, 1990,74-78

"A novel Method of pH Measurement Based on Temperature Modulation on the ISFET"

B. HU, M. DECROUX, S. JEANNERET, G.-A. RACINE and N.F. de ROOIJ

accepted for publication in:

SENSORS AND ACTUATORS,

"A novel Method of pH Measurement Based on Temperature Modulation on the ISFET"

B. HU, M. DECROUX, S. JEANNERET, G.-A. RACINE and N.F. de ROOIJ

CHAPTER 5 A novel Method of pH Measurement Based on Temperature Modulation on the ISFET

5.1 Abstract

One major problem of pH-ISFETs is the long term drift behavior. Here a novel measurement technique will be presented, by which the pH response of the sensor signal can be separated from solid-state effects which are responsible for the long term drift behavior. In this technique, the temperature of the device is modulated at a frequency of 0.5 Hz with a typical amplitude of 1°C. A synchronous detection of the signal of the ISFET gives directly the derivative of the ISFET response with respect to the temperature. When the pH temperature dependence of the measured solution is taken into account, a surface sensitivity of 0.21mV/°C/pH is obtained, in good agreement with the expected value of the surface investigated. The potential use of this technique is restricted to solutions with low pH sensitivity to the temperature. However this technique seems to be very suitable for the characterization of the sensing surface of an ISFET. With this new technique, we were able to strongly reduce the influence of the long term drift.

5.2 Introduction

The problem of the long term drift of pH-ISFETs has prevented a large scale commercialization of these devices. The progress achieved to solve the drift problem has made possible the use of these sensors for recording relatively large changes of pH but with a modest accuracy (typically in the range of a tenth of pH) as compared to their potential sensitivity. However other applications, as for instance for pH blood investigations, require a sensitivity over a small interval of pH. Unfortunately, the drift problem has severely limited the possibility to use these sensors. A lot of research has addressed this basic question, and partial solutions were proposed to attenuate the effect of the drift. It is generally admitted that this drift has a solid state origin located within the sensing layer in the case of alumina pH-ISFETs [1,2,3], a conclusion supported by the absence of any modification of the surface sensitivity of the sensing layer [4]. The slow drift of the ISFET response as function of time is explained on the basis of an additional small polarizability of the sensing layers. This additional polarizability has very large relaxation times. One possibility to attenuate the drift is to apply a square shaped voltage across the gate insulator of the ISFET [1]. Therefore the internal electric field is alternatively switched from zero to a fixed value with an expected reduction of the drift proportional to the time ratio of this square signal. Another possibility to attenuate the drift

is to use an ac modulation technique with a frequency of the sinuous signal larger than the cut-off frequency of the polarizability. It gives the opportunity to separate the drift contribution from the pH response of the ISFET. An optimal solution is found if the ac signal is generated either by the quantity to be measured, i.e. pH of the solution or by the measurement mechanism, i.e. the sensitivity of the sensing layer. Since it would be difficult to change quickly and in a reproducible way the pH of the solution we have investigated the possibility to change the sensitivity of the sensing layer by modulating its temperature. In this contribution we present for the first time, experimental results carried out with this so-called "Modulation Temperature Technique". The pH sensitive of the temperature modulation on the ISFET is based on that its temperature sensitivity is changed by pH value of the solution. Its manifestation is that the amplitude of the ac modulation signal is varied with pH.

5.3 Temperature Modulation of the sensing layer

Using the temperature and the pH characteristics of the ISFET to determine the pH of the electrolyte solution, a continuous modulation of the chip temperature is required. This temperature modulation is realized with a heating resistor. An AC voltage signal at a constant frequency and with a constant amplitude is applied to this resistor to achieve a constant temperature modulation on the ISFET, and on the interface between the electrolyte solution and the sensitive layer of the ISFET. The measuring device is composed of an ISFET, a heating resistor and a temperature sensing diode, as shown in Figure 5-1.

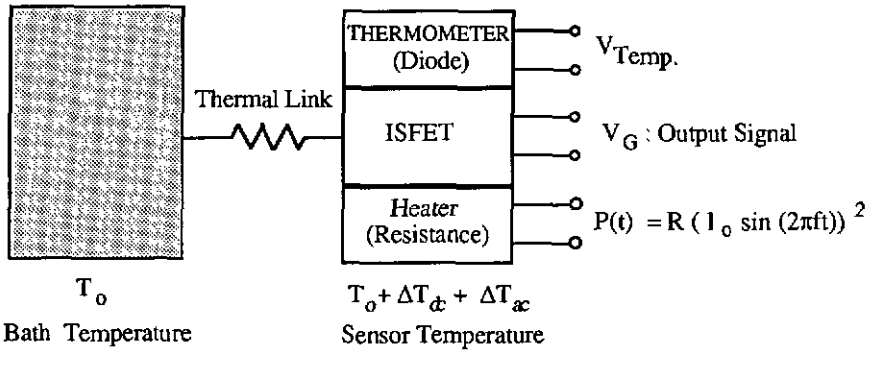

Figure 5-1. *Principle of the temperature oscillation of the ISFET.*

The device is held in a thermostated bath where the temperature is kept at a constant value of 25 °C. In the heating process a thermal power P is consumed. This thermal power is equal to the electric power provided to the resistor assuming no other sources of power being dissipated. The heat transmission in the measuring chamber is illustrated in Figure 5-1.

From conservation of the thermal energy, the thermal power transferred to the system can be expressed by [8]:

$$P = C\frac{d\Delta T}{dt} + K\,\Delta T \qquad (5\text{-}1)$$

where C is the heat capacity of the whole device, $\Delta T = T - T_0$, T temperature of the device, T_0 the bath temperature, K the thermal link of the device. The power P is modulated with the alternating potential on the heating resistor at the frequency ωt. It is calculated by:

$$P(t) = \frac{U_0^2}{R}\sin^2 \omega t = \frac{U_0^2}{2R} - \frac{U_0^2}{2R}\cos 2\omega t = P_1 - P_2\,(2\omega t) \qquad (5\text{-}2)$$

where R is the resistance of the heater, U_0 the amplitude of the alternating potential applied to the resistor. The first term of the solution in equation (5-2) can be considered as a mean power $P_1 = \frac{U_0^2}{2R}$ which generates a temperature offset ΔT_{DC} over the bath temperature T_0 on the device, such as:

$$P_1 = C\frac{d\Delta T_{DC}}{dt} + K\,\Delta T_{DC} \qquad (5\text{-}3)$$

The solution $\Delta T_{DC}(t)$ that satisfies this differential equation is found:

$$\Delta T_{DC} = \frac{P_1}{K}\,(1 - e^{-Kt/C}) \qquad (5\text{-}4)$$

This offset will be constant in the steady state when thermal equilibrium in the measuring cell is reached. The temperature offset is calculated taking the limit $t \S \infty$:

$$\Delta T_{DC} = \frac{P_1}{K} = \frac{U_0^2}{2RK} \qquad (5\text{-}5)$$

This equation shows that the temperature offset ΔT_{DC} depends on the amplitude of the alternating potential realized on the resistor in order to obtain the expected temperature modulation of the ISFET.

The second part of the power transmitted to the system P_2 is modulated at twice the frequency of the AC voltage with an amplitude P_1. A synchronous detection of the temperature called ΔT_{AC} will be produced based on mean temperature T of the device. Substituting P_2 into equation (5-1), this temperature modulation ΔT_{AC} can be calculated by:

$$P_2 = P_1 \cos 2\omega t = C \frac{d(\Delta T_{AC})}{dt} + K \Delta T_{AC} \qquad (5\text{-}6)$$

Solving this equation, a common solution for ΔT_{AC} is obtained:

$$\Delta T_{AC} = \frac{P_1}{(4\omega^2C^2+K^2)} (2\omega C\sin(2\omega t) + K\cos(2\omega t)) + Ae^{-Kt/C} \qquad (5\text{-}7)$$

Considering that the measurement is performed in a steady state, $Ae^{-Kt/C}$ becomes zero. We introduce:

$$tg\varphi = \frac{2\omega C}{K} \qquad (5\text{-}8)$$

Substituting equations (5-8) into equation (5-7), it can be written as:

$$\Delta T_{AC} = \frac{P_1}{\sqrt{4\omega^2C^2+K^2}} (\cos(2\omega t - \varphi)) \qquad (5\text{-}9)$$

where φ is the phase shift between the ac response of the ISFET and the ac power.

In this equation C and K are constant, the ΔT_{AC} amplitude $\frac{P_1}{\sqrt{4\omega^2C^2+K^2}}$ is proportional to P_1 and inversely proportional to the frequency ω. If the potential is limited by the voltage source, the frequency of the potential should be low to obtain enough signal amplitude. Another restriction on the potential is that it will increase ΔT_{DC} which is not desirable. This relationship between amplitude of ΔT_{AC} and offset of ΔT_{DC} can be obtained from equation (5-5) and (5-9) and shown as:

$$\Delta T_{AC} = \frac{\Delta T_{DC}}{\sqrt{4\omega^2C^2/K^2+1}} \qquad (5\text{-}10)$$

From this equation we can see that when $\omega \ll K/C$, the amplitude of ΔT_{AC} is similar to the ΔT_{DC}. This condition implies a small heat conduction relative to the heat capacity.

5.4 The measuring mechanism

a) pH and temperature sensitivity

When the ISFET using alumina as the pH layer is operated at a constant current mode with a constant drain to source voltage V_D, the reference electrode (gate) to the source voltage V_G is used as the measurement signal of the ISFET. In the linear operation range V_G is given by [5]:

$$V_G = \frac{I_D L}{\mu_n W C_o V_D} + E_{ref} - \Psi_o + \chi - \frac{1}{q}\Phi_{Si} - \frac{Q_{ss}}{C_o} + 2\Psi_B - \frac{Q_B}{C_o} + \frac{1}{2} V_D \qquad (5\text{-}11)$$

where μ_n denotes the electron mobility, W the channel width, L the channel length, C_o the insulator capacitance per unit area, I_D the drain-source current, E_{ref} denotes the reference electrode potential relative to vacuum, Ψ_o the potential difference between the insulator surface and the bulk of the solution (surface potential), χ the surface dipole potential at the insulator/solution interface, $\frac{1}{q}\Phi_{Si}$ the silicon work function, Q_{ss} the charge inside the insulator, Q_B is the charge per unit area in the silicon surface at inversion and Ψ_B the Fermi potential difference between doped and undoped silicon. The pH-sensitivity mechanism of an ISFET is based on a surface reaction. The surface potential modulated by pH of the electrolyte solution at the insulator-electrolyte interface, induces a pH sensitivity of the ISFET. The surface potential Ψ_o is expressed by [4]:

$$\Psi_o = \frac{\beta}{\beta+1} \frac{2.303kT}{q} (pH_{pzc} - pH) \qquad (5\text{-}12)$$

where β is a dimensionless sensitivity parameter, k is the Boltzmann constant, T is the absolute temperature and pH_{pzc} is the pH at point of zero charge of the oxide material. From equations (5-11) and (5-12) the pH sensitivity S can be derived as:

$$S = -\frac{\partial \Psi_o}{\partial pH} = 2.303 \frac{\beta}{\beta+1} \frac{kT}{q} = \frac{\partial V_G}{\partial pH} \qquad (5\text{-}13)$$

The AC surface potential induced by the temperature modulation ΔT_{AC} and the temperature dependence of the surface potential Ψ_o are given by:

$$\left(\frac{\partial \Psi_o}{\partial T}\right)_{pH} \Delta T_{AC} \text{ and}$$

$$\left(\frac{\partial \Psi_o}{\partial T}\right)_{pH} = 2.303 \frac{k}{q} \frac{\beta}{\beta+1} \left[\left(1+\frac{T}{\beta(\beta+1)} \frac{\partial \beta}{\partial T}\right)(pH_{pzc}-pH) + T \frac{\partial pH_{pzc}}{\partial T}\right] \quad (5\text{-}14)$$

The term $\frac{\partial \beta}{\partial T}$ is expressed by [5]:

$$\frac{\partial \beta}{\partial T} = \frac{\beta}{T}\left(\frac{\Delta H_{a2}-\Delta H_{a1}}{2RT} - 1\right) \quad (5\text{-}15)$$

where ΔH_{a1} and ΔH_{a2} are the enthalpy changes for the surface proton dissociation reactions [6] and R is the molar gas constant.

However the whole change of the surface potential includes also the change of the pH with the temperature i.e. $\Psi_o = \Psi_o(T, pH(T))$. Assuming that the temperature of the solution at the interface and of the sensing layer are the same, we can apply the following correction to get the true pH sensitivity of the temperature modulation sensing layer.

$$\frac{d\Psi_o}{dT} = \left(\frac{\partial \Psi_o}{\partial T}\right)_{pH} + \frac{\partial \Psi_o}{\partial pH} \frac{\partial pH}{\partial T} \quad (5\text{-}16)$$

As a consequence, a low temperature dependence of the solution pH is required in order to avoid an important correction to obtain the pH sensitivity of the layer.

The pH sensitivity of the AC surface potential induced by the temperature modulation ΔT_{AC} is derived by:

$$\frac{\partial^2 \Psi_o}{\partial T \partial pH} = -2.303 \frac{k}{q} \frac{\beta}{\beta+1}\left(1+\frac{T}{\beta(\beta+1)} \frac{\partial \beta}{\partial T}\right) \quad (5\text{-}17)$$

For large ß parameters (Nernstian limit) the sensitivity at 300 °K is 199 μV/(K pH) whereas for a real surface the deviation from the Nernstian behavior allows to determine ß.

In practice, V_G is measurement parameter. Using equation (5-11), the temperature derivative of V_G can be expressed as:

$$\frac{\partial V_G}{\partial T} = -\frac{\partial \Psi_o}{\partial T} + \frac{\partial V_{SI}}{\partial T} \quad (5\text{-}18)$$

where $V_{SI}(T) = 2\Psi_B - \frac{Q_B}{C_o} + \frac{I_D L}{\mu_n W C_o V_D} + \frac{1}{2}V_D + \chi - \Phi_{Si} - \frac{Q_{ss}}{C_o}$.

$V_{SI}(T)$ is a temperature dependent solid state contribution of the ISFET. According to equation (5-16), the output signal can be expressed as:

$$\frac{dV_G}{dT} = -\left(\frac{\partial \Psi_o}{\partial T}\right)_{pH} - \frac{\partial \Psi_o}{\partial pH}\frac{\partial pH}{\partial T} + \frac{\partial V_{st}}{\partial T} \qquad (5\text{-}19)$$

Since the MAOSFET (Metal Alumina Oxide Semiconductor Field Effect Transistor) has a similar temperature dependence in the solid state part as the ISFET when they are fabricated on one wafer, the MAOSFET can be used to compensate for the temperature effect of the solid state part of the ISFET. The temperature sensitivity of the surface potential can be thus obtained [3]:

$$\left(\frac{d\Delta V_G}{dT}\right)_m = -\left(\frac{\partial \Psi_o}{\partial T}\right)_{pH} + \frac{\partial \Psi_o}{\partial pH}\frac{\partial pH}{\partial T} \qquad (5\text{-}20)$$

b) time behaviour

With normal measurement techniques, the pH measurement with the ISFET drifts with exposure time. This base-line drift of the ISFET is mainly determined by the solid state part of the sensor [1,2,3]. The drift phenomenon in alumina ISFETs, which is attributed to solid state bulk polarization of the alumina layer, was found by measurements on the MAOS capacitors. Therefore E_{ref}, Ψ_o and χ in equation (5-11) can be considered to be independent of the exposure time. In the first hours of exposure to the solution the empirical law [1] for the bulk polarization is expressed as:

$$\chi_a (t > 0) = \chi'_a (T) \ln\left(\frac{t}{t_o} + 1\right) \qquad (5\text{-}21)$$

where χ_a is bulk polarizability of the alumina, the value of t_o is determined by the experimental procedure. A relation between the bulk polarizability χ'_a (T) and temperature T can be expressed as:

$$\chi'_a (T) = \chi_o e^{-U_a/kT} \qquad (5\text{-}22)$$

where U_a is an activation energy. The temperature dependence of the bulk polarizability is derived from equation (5-22):

$$\frac{\partial \chi_a}{\partial T} = \chi'_a (T) \frac{U_a}{kT^2} \ln\left(\frac{t}{t_o} + 1\right) \qquad (5\text{-}23)$$

Such a bulk polarization is equivalent to a surface charge at the alumina-oxide interface that is included in the charge Q_{ss} inside the insulator:

$$Q_{ss} = Q_{ox} + \varepsilon_o \chi_a E_a \qquad (5\text{-}24)$$

where ε_o is the permittivity of free space and E_a is the electric field in the alumina layer. Therefore the charge inside the insulator contributes to the time dependence of the V_G. The base-line drift of the ISFET can therefore be derived as:

$$\frac{\partial V_G}{\partial t} = -\frac{1}{C_o}\frac{\partial Q_{ss}}{\partial t} \tag{5-25}$$

When the ISFET is modulated by the temperature variation during pH measurement, the output signal is also dependent on the exposure time. Based on equation (5-25) the derivation of the time dependence of V_G as function of the temperature modulation can be obtained by:

$$\frac{\partial^2 V_G}{\partial T \partial t} = -\frac{1}{C_o}\frac{\partial^2 Q_{ss}}{\partial T \partial t} + \frac{1}{C_o^2}\frac{\partial C_o}{\partial T}\frac{\partial Q_{ss}}{\partial t} \tag{5-26}$$

In this equation the temperature dependence of the insulator capacitance per unit area C_o can be derived by :

$$\frac{\partial C_o}{\partial T} = \frac{\partial}{\partial T}\left(\frac{\varepsilon_{ox}}{d}\right) = \frac{1}{d}\frac{\partial \varepsilon_{ox}}{\partial T} \tag{5-27}$$

where ε_{ox} is the permittivity of oxides (silicon dioxide and alumina) and d is the the gate oxide thickness. Note the thermal expansion effects in oxides are considered to be negligible. Since the permittivity ε_{ox} is related to the total bulk polarization χ_{ox} of the oxide by the relation: $\varepsilon_{ox} = \varepsilon_o \chi_{ox} - \varepsilon_o$, we can have:

$$\frac{\partial \varepsilon_{ox}}{\partial T} = \varepsilon_o \frac{\partial \chi_{ox}}{\partial T} \tag{5-28}$$

where ε_o is the dielectric constant. According to a previous study on the MOSFET the capacitance per unit area for silicon dioxide is independent on temperature [14]. This temperature effect acts only on the alumina layer for ISFET.

According to equations (5-21) and (5-23), the terms $\frac{\partial Q_{ss}}{\partial t}$ and $\frac{\partial^2 Q_{ss}}{\partial T \partial t}$ of equation (5-26) are derived as:

$$\frac{\partial Q_{ss}}{\partial t} = \frac{\partial Q_p}{\partial t} = \varepsilon_o E_a \frac{\partial \chi_a}{\partial t} = \varepsilon_o E_a \chi'_a(T)\frac{1}{t+t_o} \tag{5-29}$$

$$\frac{\partial^2 Q_{ss}}{\partial T \partial t} = \varepsilon_o E_a \chi'_a(T)\frac{U_a}{kT^2}\frac{1}{t+t_o} \tag{5-30}$$

With an alternating thermal excitation the drift effect of the bulk polarization is frequency dependent as a function of the relaxation time. In a generalized model, Debye equations as well as the plotted results [13] give the relation between relaxation time and permittivity which affect on the polarization. For the attempted mechanism of bulk polarization the distribution of the relaxation times has to show a maximum for one typical frequency. Therefore at a frequency which is low enough or high enough, the bulk polarization could be independent of drift. In the simple model used in equations (5-26), the time constant t_0 can be interpreted as the inverse of a cut-off frequency f_0. Equation (5-26) reduces to:

$$\frac{\partial^2 V_G}{\partial T \partial t} = \varepsilon_o E_a \frac{\chi_o \exp(-U_a/kT)}{C_o} \left(\frac{1}{C_o} \frac{1}{d} \frac{\partial \varepsilon_{ox}}{\partial T} - \frac{U_a}{kT^2} \right) \frac{f_0}{1 + f_0 t} \qquad (5\text{-}31)$$

With a phase sensitive detection of the thermal excitation, the drift contribution reduces to:

$$\Delta V_G \cong \varepsilon_o E_a \frac{\chi_o \exp(-U_a/kT)}{C_o} \left(\frac{1}{C_o} \frac{1}{d} \frac{\partial \varepsilon_{ox}}{\partial T} - \frac{U_a}{kT^2} \right) (1 + f_0 t)^{-1} \frac{f_0}{f} \Delta T_{AC} \qquad (5\text{-}32)$$

This equation is dependent on the excitation frequency f. If measurements are done above this cut-off frequency, the drift contribution of V_{st} will be reduced at least by the function $\frac{f_0}{f}$.

5.5 Experimental

Combined sensors are obtained with a pH-ISFET, a temperature sensing diode and a heater. In order to simplify the fabrication process and to use existing chips, an ISFET, a heating resistor and a diode are fabricated on individual silicon chips. The pH-ISFETs with an alumina pH sensitive layer are fabricated using a standard process [9]. A resistor of 1.5 kΩ is used as the heater. A diffused junction diode is used as a temperature sensing element. The ISFET and the temperature sensing diode were glued on to the heating resistor chip with epoxy. The whole device was bonded and encapsulated on a support with epoxy, only the sensitive part of the ISFET was exposed to the test solution. The temperature on the ISFET and the diode is considered to be equal.

The ISFET was operated in the constant current mode with a constant drain-source voltage, using a special amplifier system. The voltage (V_G) between the reference electrode and the source was used as an output parameter. A function generator supplied a

signal to the heating resistor with an alternating potential (amplitude 0-30 V) and a synchronous signal for the reference channel of the lock-in amplifier. Thus the signal of the ISFET was modulated by the temperature variation introduced by the heating resistor and detected by a lock-in amplifier. The recorded output of the lock-in amplifier is proportional to the temperature sensitivity of the gate to source voltage dV_G/dT. The amplitude of the temperature modulation was controlled at about 1 °C by adjusting the voltage on the heater, and was measured by the temperature sensing diode. However, lowering the frequency of excitation and detecting synchronously the temperature modulation of the ISFET signal V_G at twice the frequency poses some instrumentational problems. This lower limit depends on the limits of the lock-in amplifier used for the signal detection. Therefore a frequency of 0.25 Hz for the heating potential has been chosen. The output voltage of V_G with a frequency of 0.5 Hz was measured by a lock-in amplifier at its lower limit. The amplitude of the alternating temperature variation was adjusted at about 1 °C.

When the heat resistor was connected to the voltage source, the temperature ΔT_{DC} stabilized in 3 minutes. The temperature offset ΔT_{DC} is about 3.3°C. Since the elements of the device were fabricated on individual chips, the size of the device and the response time of heat were limited. If an integrated chip was made, the device could be operated at a condition with higher frequency due to the short heat response time and decreased thermal losses. The measuring technique would be easier.

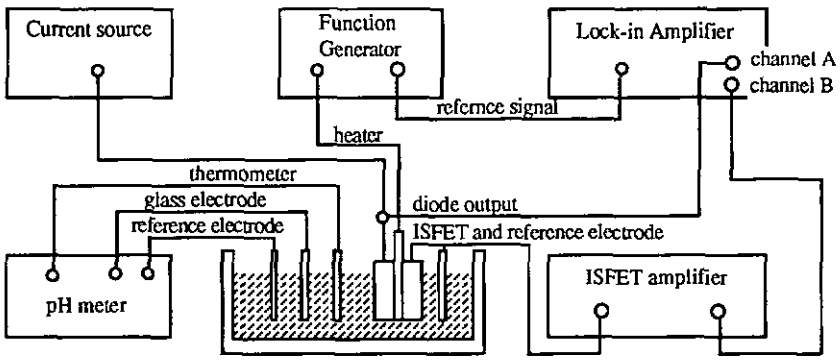

Figure 5-2. *The setting of the measuring system.*

The signal of the diode was detected by the same lock-in amplifier. All output signals, i.e. from the ISFET amplifier, the voltage of the diode and from the lock-in amplifier were recorded.

Standard pH buffer solutions (MERCK) from pH 2 to pH 9 and a HCl-Tris buffer solution (pH 7.6) were used. The pH values of the HCl-Tris solutions were changed by adding HCl and NaOH. The pH values of the solutions were measured in function of bath temperature by an independent pH meter with a glass electrode (Metrohm) and a separate double-junction reference electrode (Metrohm). The glass electrode and reference electrode were recalibrated with MERCK buffers solutions over the whole measurement temperature range. Figure 5-2 shows a diagram of the whole measuring system.

5.6 Results and Discussions

The temperature sensitive diodes were tested in the temperature range from 10 °C to 30 °C. They had a sensitivity of 2.3 mV/°C when operated at a current of 100 μA . In the measuring system the ISFET response with respect to the temperature modulation at a frequency of 0.5 Hz with a typical amplitude of 1 °C was observed at different pH values. Since the amplitude of the temperature modulation is quite small and the reference electrode was located far away from the device, the temperature of the reference electrode can be considered as to be independent of the temperature modulation.

A more important and interesting result is the long term drift measurement. This measurement was performed in the first hours where the ISFETs usually show the largest drift. Figure 5-3 shows the resulting curves including the signal of the ISFET with the variations made by the heater and the signal measured by a lock-in amplifier on the alternating signal of V_G.

During the measurement the mean temperature of the device was very stable. The amplitude of the temperature modulation was about 1 °C with a frequency of 0.5 Hz. This figure shows a baseline drift rate of the ISFET is more than 1.2 mV/hr. The synchronous detection of the alternating signal of V_G is constant with time. This result presents the drift term expressed in equation (5-26). According to equations (5-27) and (5-28) the drift terms in this equation are dependent on the bulk polarization of the alumina. Since the ISFET is operated in an alternating temperature excitation, during measurements the bulk polarization can not follow the temperature modulation at the applied frequency. An explanation for this is that the value t_0 measured by previous studies [1,2,11,12] at room temperature ranges from 15 seconds to several minutes. The corresponding relaxation time is much greater than t_0. Comparing the curves of Debye equations the time dependence of the permittivity of alumina is so small as to be negligible in this measuring condition. And the value of the temperature dependence of the insulator capacitance per unit area C_0 is very small at room temperature. The drift with temperature modulation can be considered to be undetectable. The result of equation (5-32) is therefore in good

agreement with a detected drift equal to zero according to the function of the lock-in amplifier.

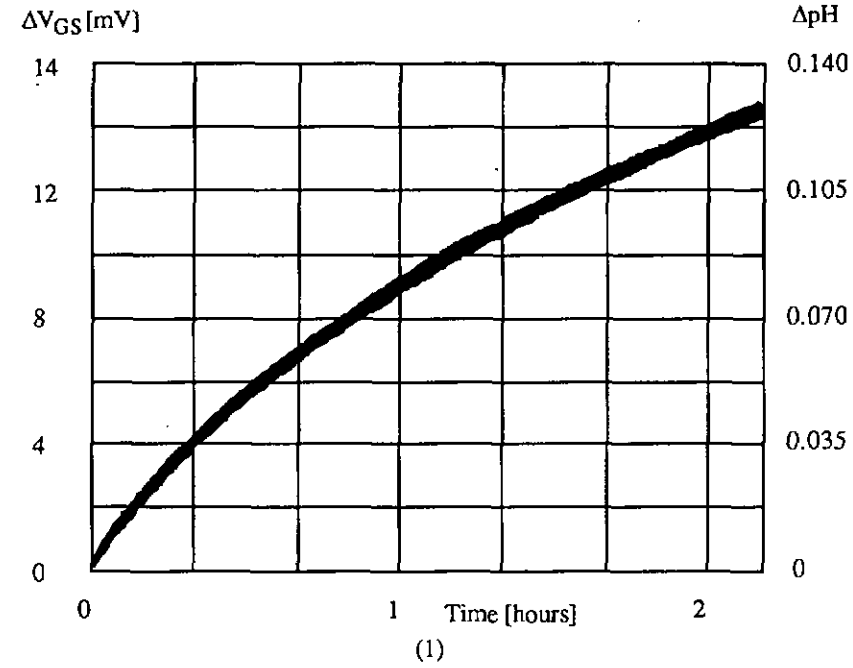

Figure 5-3. *Comparison of the long-term drift between (1) the normal drift of the ISFET with the alternating variation caused by temperature change of 1 °C with a frequency of 0.5 Hz, (2) the drift of the alternating signal measured by a lock-in amplifier .*

Table 5-1. *Overview of the results in two buffer solution. The temperature sensitivity of an IGFET is -1.455 mV/°C.*

pH (25 °C) [1]	$(dV_G/dT)_m$ (mV/°C) [1]	$\partial pH/\partial T$ (pH/°C) [1]	$S*\partial pH/\partial T$ (mV/°C) [2]	$\partial V_G/\partial T$ (mV/°C) [2]	$-\partial \Psi_o/\partial T$ (mV/°C) [2]
Device No.7 in HCl-Tris buffer. S = 57.0 mV/pH [1] at 25°C					
7.092	-1.470	-0.02711	-1.545	0.075	1.530
7.405	-1.422	-0.02732	-1.557	0.135	1.590
8.177	-1.337	-0.02821	-1.608	0.271	1.726
9.105	-1.070	-0.02757	-1.571	0.501	1.956
Device No.7 in Merck buffer. S = 56.7 mV/pH [1] at 25°C					
2.008	-0.957	0.00276	0.156	-1.113	0.342
2.992	-0.986	0.00042	0.023	-1.009	0.446
4.007	-0.819	0.00090	0.051	-0.870	0.585
5.064	-0.621	0.00000	0.000	-0.621	0.834
6.082	-0.371	0.00112	0.063	-0.435	1.020
7.034	-0.364	-0.00498	-0.283	-0.081	1.374
8.934	-0.288	-0.00850	-0.482	0.195	1.650
Device No.10.1 in Merck buffer. S = 56 mV/pH [1] at 25°C					
4.007	-0.619	0.00090	0.045	-0.664	0.791
6.082	-0.257	0.00112	0.056	-0.313	1.142
7.034	-0.228	-0.00498	-0.250	0.022	1.477
8.934	-0.126	-0.00850	-0.427	0.301	1.756

S is the pH sensitivity.

1. measured.

2. calculated.

The ISFETs had a normal pH sensitivity of 56.7 mV/pH measured in standard pH buffer solution (MERCK) and of 57.0 mV/pH measured in HCl-Tris buffer solution from pH 2 to pH 9 at 25 °C with standard method.

According to equation (5-20), results of the AC temperature dependence of the surface potential were obtained by that the AC signals of the ISFET were compensated for the temperature dependence of the IGFET. In order to calculate the difference of the temperature dependences of the ISFETs and of the IGFETs, the temperature dependence of IGFETs was measured. As a result, a mean value of $\partial V_G/\partial T$ = -1.455 mV/°C was observed in a temperature range from 10 °C to 30 °C for the IGFETs fabricated on the same wafer as ISFETs. The results in terms of equation (5-19) and (5-20) were measured in different pH values of the HCl-Tris buffer solution and the pH standard buffer solutions of MERCK and calculated, as shown in Table 5-1.

Using these results the pH dependence of the $\frac{\partial V_{GS}}{\partial T}$ was plotted in Figure 5-4. From these results we obtain:

$$-\frac{\partial^2 \Psi_o}{\partial T \partial pH} = \frac{\partial^2 V_G}{\partial T \partial pH} = 0.204 \pm 0.081 \text{ mV/(°C·pH)} \qquad (5\text{-}33)$$

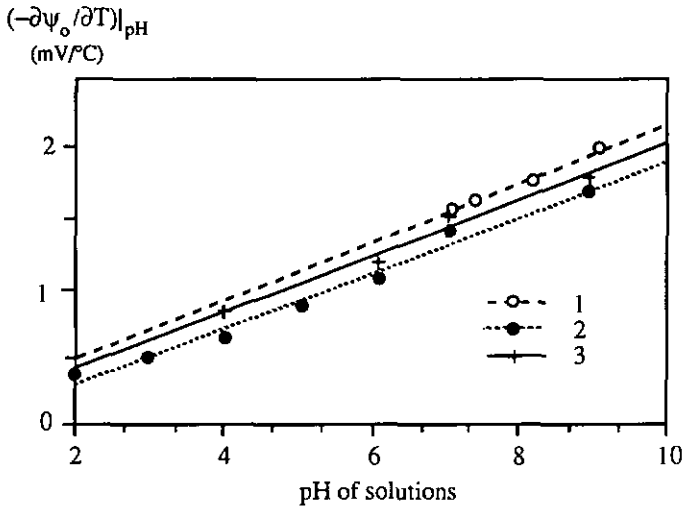

Figure 5-4. *The pH dependence of the temperature derivative of the surface potential at 25°C. (o) ISFET No.7 in HCl-Tris buffer solution, sensitivity 0.210 mV/(°CpH), (•) ISFET No.7 in MERCK buffer solution, sensitivity 0.201 mV/(°CpH), and (+) ISFET No. 10 in MERCK buffer solution, sensitivity 0.202 mV/(°CpH).*

According to equation (5-19), the drain current I_D can shift the temperature dependence of the ISFET, but can't change its sensitivity. The same measurement with a

different drain current I_D was performed in two different electrolyte solutions. We found that the current I_D made an offset of $\frac{\partial V_G}{\partial T}$ at different pH, but that the slope was always the same.

As a theory of the temperature dependent pH sensitivity of the ISFET shows the same result as the pH sensitivity of the temperature dependent V_G, as expressed by:

$$\frac{\partial}{\partial T}\left(-\frac{\partial \Psi_0}{\partial pH}\right) = 2.303 \frac{k}{q} \frac{\beta}{\beta+1}\left(1+\frac{T}{\beta(\beta+1)}\frac{\partial \beta}{\partial T}\right) \qquad (5\text{-}34)$$

the measurement of the temperature dependent pH sensitivity can be used to calibrate our results. Based on this theory, the pH sensitivities at different temperatures were measured and the results are shown in Figure 5-5. The slope of the line passing through these points, which expresses the term $\frac{\partial^2 \Psi_0}{\partial pH \partial T}$, is - 0.20 mV/pH°C. It corresponds to the result $\frac{\partial^2 V_G}{\partial T \partial pH}$ as well as - $\frac{\partial^2 \Psi_0}{\partial T \partial pH}$. Therefore we prove experimentally that the temperature dependence of the ISFETs is sensitive to the pH of the solution. This sensitivity can be determined when a correction for the pH temperature dependence of the measured solution is made.

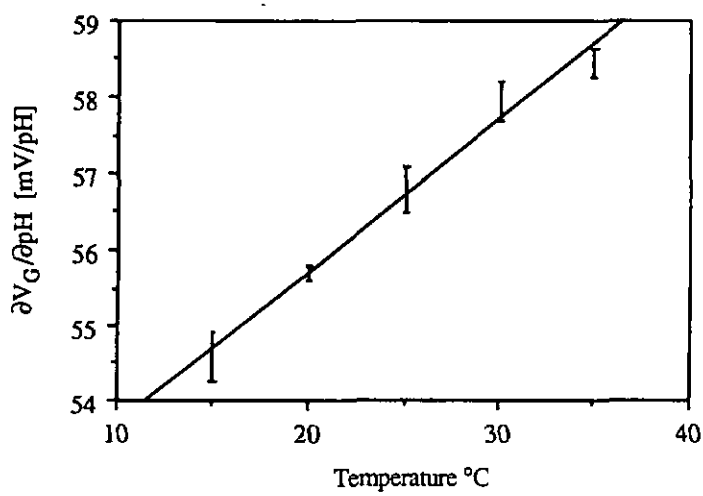

Figure 5-5. *The temperature dependence of the pH sensitivity for an ISFET. The slope is 0.2 mV/pH°C.*

The results shown in Figure (5-4) are in good agreement with the expected value for the alumina surface. The calculation using equations (5-14) and (5-15) with one of these results: $\beta = 27.08$ corresponding to a pH sensitivity of 57.0 mV/pH observed in HCl-Tris

buffer solution and the surface sensitivity of 0.210 mV/(pH°C), shows a results of the entropy charge ΔH_{a2}-ΔH_{a1} = 7.6 RT. This result is similar to a previously investigated result ΔH_{a2}-ΔH_{a1} = (7.8 ± 1.4)RT [3,7]. However, the sun of the enthalpy charges ΔH_{a2}+ΔH_{a1} could not be calculated, due to errors of offset of these measurements.

5.7 Conclusions

When the pH temperature dependence of the measured solution is taken into account, a surface sensitivity of about 0.21 mV/°C/pH was obtained. It is concluded that pH of the solution can be measured with this new method. This value is comparable with the results measured by the normal method [3,7] and corresponds with the calculated value. Using the new method, the influence of long term drift can be strongly reduced. This new technique seems to be very suitable for characterization of the sensing surface of an ISFET and application to studies on the surface ionization enthalpies of materials. However, the measurements should be done in solutions with a constant mean temperature.

The pH temperature dependences are specific for each solution, the measurements in the HCl-Tris buffer solution and Merck standard buffer solutions. But similar values of pH sensitivity were obtained after compensation for the term $\frac{\partial pH}{\partial T}$. Two suitable applications are: a) measurements preformed in a small range of the pH, where the pH temperature dependences can be considered as to be linear; b) where the sample has a well known temperature dependence for the pH. For example in the pH measurement of blood it is quite important for the biomedical applications. The relationship between pH of the blood and temperature is given by [9]:

$$pH(T) = pH(T_o) + (T-T_o) * (a\,(b - pH(T_o)) - c) \qquad (5\text{-}35)$$

where T_o = 37 °C, a = 0.0065, b = 7.4 and c = 0.0146.

Using this equation we can easily calculate the temperature sensitivity of the blood pH. Therefore using this method to measure pH of the blood the errors made by the drift of the ISFET can be avoided and recalibrations during measurement are not needed.

5.8 References

[1]. H.C.G. Ligtenberg, Thesis University of Twente, The Netherlands, 1987.

[2]. C. Arnoux, Thesis, University of Neuchâtel, Switzerland, 1988.

[3]. H.H. van den Vlekkert, Thesis, University of Neuchâtel, Switzerland, 1988.

[4]. L. Bousse, N.F. de Rooij, and P. Bergveld, IEEE Trans. Electron Device, Vol. ED-30, No. 10, 1983, 1263-1270.

[5]. J. Janata and R.J. Huber, In H. Freiser (Ed.) Ion-selective electrode in analytical chemistry, Vol. 2, Plenum Press, 1980, 107.

[6]. L. Leistiko, Physica Scripta, Vol. 18, 1978, 445.

[7]. H.H. van den Vlekkert, L. Bousse, and N.F. de Rooij, J. Colloid and Interface Science, Vol. 122, No.2, 1988, 336-345.

[8]. D. Halliday and R. Rosnick, in Fundamentals of Physics, Ed. John Wiley & Sons Inc., 1986.

[9]. H.H. van den Vlekkert and N.F. de Rooij, Analusis, Vol. 16, No. 2, 1988, 110-119.

[10]. G.M. Sakharova, A.G. Ustinov, S.A. Gasparyan, and E.A. Limarenko, Biomedical Engineering (New York), Vol. 21, No. 1, 1987,10-13.

[11]. Ch. Arnoux, R. Buser, M. Decroux, H.H. van den Vlekkert and N.F. de Rooij, Proc. Transducers'87, Tokyo, Japan, 1987, 751-754.

[12]. A.P. Gnadinger and W. Rosenzweig, J. Electrochem. Soc. Vol. 121, No. 5, 1974, 700-705.

[13]. I. Bunget and M. Popescu, Physics of Solid Dielectrics, Elsevier, 1984.

[14]. L. Vadasz and A.S. Grove, IEEE Tran. Electron Devices, Vol. ED-13. No.12, 1966, 863-866.

[15]. L. Leistiko, Physica Scripta, Vol. 18, 1978, 445.

CHAPTER 6
Reduction of the Drift Rate of the pH-ISFET with Al_2O_3 as a pH Sensitive Material

CHAPTER 6 Reduction of the Drift Rate of the pH-ISFET with Al_2O_3 as a pH Sensitive Material

6.1 Abstract

In this chapter the reduction of the drift rate which is a major problem of pH-ISFETs, is discussed for the pH-ISFET with alumina Al_2O_3 as the pH sensitive layer. The assumption that the hydrogen in the alumina layer is responsible for the drift is confirmed by drift measurements on the pH-ISFET and MAOSFET with an alumina layer deposited in a low hydrogen content. From these measurements, we conclude that a reduction of the drift rate can be obtained by diffusion of aluminum atoms during the annealing procedure.

6.2 Introduction

The characteristics of the long term drift in pH measurement with ISFETs has been mentioned in chapters 2, 3 and 4. This drift behavior influences the accuracy of the measurement and impedes the application of ISFETs, especially in the biomedical field where very high accuracy is needed and recalibrations have to be avoided. Over the past years several materials as the pH sensitive layer on the ISFET have been investigated with respect to their drift behavior, such as SiO_2, Si_3N_4, Al_2O_3 and Ta_2O_5. The ISFET with Al_2O_3 as a sensitive layer shows a better stability than do the ISFET with SiO_2 and Si_3N_4 [1]. The drift rate of an ISFET with Si_3N_4 is about 0.6mV/h and with Al_2O_3 is about 0.3 mV/h after 10 hours of stabilization. The ISFET with SiO_2 was not stable at all. Matsuo et al. [2] compared SiO_2, Si_3N_4, Al_2O_3 and Ta_2O_5 materials where they found a drift rate of 1 mV/h for Si_3N_4, and a drift rate of 0.1 - 0.2 mV/h for Al_2O_3 and Ta_2O_5 after 1000 min of operation at pH 7. This value corresponds to the result which was observed on the ISFET with an Al_2O_3 layer in HCl-Tris buffer solution [3]. Therefore, Al_2O_3 and Ta_2O_5 are good materials to use as the pH sensitive layer for ISFETs, and the drift rate of the ISFET with Al_2O_3 is quite reproducible and independent of the fabrication and the measuring technique.

In order to understand the drift behavior, the mechanism of the base-line drift has been studied during the last several years. The drift behavior of the ISFET with SiO_2 can be explained by the theory of buried sites at the periphery of the electrolyte interface as far as chemical drift is concerned [4].

The drift of the ISFET with alumina as the pH sensitive layer is mainly caused by solid state effects that are present both on the ISFET and on the MAOSFET (metal alumina silicondioxide semiconductor field effect transistor) structures. This has been observed by a similar drift behavior for both ISFETs and MAOSFETs [5,6]. Further investigation of the MAOS structure which had been subjected to bias temperature time stress experiments (BTTS), showed that the drift is attributable to a solid state bulk polarization of the alumina layer [5].

In a similar study, charge injection in metal-Al_2O_3-SiO_2-silicon (MAOS) structures was investigated by Balk and Stephany [7] using the capacitance-voltage technique. They found that the threshold voltage shifts with positive voltage are roughly logarithmic with time. They claim that induced charge, trapped in the alumina layer causes the drift.

Another similar study confirmed that the drift is a solid state effect and is localized within the alumina layer by Dr. Arnoux [6]. In this study the alumina layer was investigated. The results show that this layer is poly-crystalline with a γ-Al_2O_3 structure and that the typical grain size is 30-50 nm. The γ-structure of Al_2O_3 is formed by a face centered cubic closed-packed lattice (spinel structure) of oxygen atoms, where aluminum ions do not completely fill up all the interstitial spaces. The drift of the flatband voltage was then interpreted as a diffusion of positive charges through the Al_2O_3 layer. According to this theory the first assumption was that the hydrogen ions could be responsible for the drift, because hydrogen was used during the fabrication process. It was concluded that the drift is attributed to two components which are mainly the bulk polarization due to H^+ ions in the interstitial position of the γ-Al_2O_3 structure and a small component may be due to migration of the other charges along grain boundaries.

A considerable amount of the research has been directed towards analyzing the drift problem of the alumina layer. A reduction of the drift rate of the ISFET with alumina was reported for ISFETs encapsulated with glass by the anodic bonding method by Dr. van den Vlekkert [9]. A later study showed that this reduction was caused only by the high temperature treatment during the anodic bonding [10]. It was concluded that the drift is caused by a diffusion of the hydrogen along the grain boundaries. The annealing alters the trap density.

Following these investigations, reduction of the drift with low hydrogen content manufacturing process and annealing treatment has been studied. In this study two steps were performed. In the first step a normal thickness (600 Å) of alumina was used [11]. The alumina layer was deposited with lower hydrogen concentration and the ISFETs with the gate area covered by aluminum during various annealing treatments were compared. The results showed that the long term drift of the MAOSFETs with low H_2 alumina was evidently reduced, but the drift reduction of the ISFETs with low H_2 could be observed

only after the annealing treatment with the gate area covered by aluminium. It was confirmed that the hydrogen ions are responsible for the drift of the MAOSFET. It was concluded that the hydrogen ions could diffused or migrate along the grain boundaries of the alumina layer and the anneal could be the remedy because the grain size is enlarged. It was proposed to make the alumina layer thicker with lower hydrogen content, in order to avoid the diffusion or migration of the ions. In accordance with this theory the second step with a thicker alumina and low hydrogen content was tried. The differences between this study and studies of Dr. Arnoux and Dr. van den Vlekkert were that the drift of the alumina layer with low hydrogen content was observed directly on the pH-ISFETs and the MAOSFETs, and the effects of the different thicknesses of alumina layer and the anneal with the gate area covered by aluminium at different temperature on the ISFETs were observed. We obtained that the drift of the ISFETs could be reduced by decrease of hydrogen content in the alumina with a diffusion of aluminum ions. The effects of this diffusion were filling up the interstitial spaces in alumina, increasing grain sides and decreasing grain boundaries, and preventing the migration of H^+ ions.

In this chapter, the method of differential measurements for reducing drift rates will also be discussed.

6.3 Experimental

The fabrication of ISFETs and MAOSFETs for comparison of the different H_2 concentration in the Al_2O_3 layer followed a standard procedure upto deposition of the alumina layer [3]. The alumina layer was deposited in an APCVD reactor at 900 °C using the $AlBr_3$ - H_2 - NO system [8] with the following chemical reactions:

$$2\,NO + 2\,H_2 \overset{>700°C}{\Leftrightarrow} N_2 + 2\,H_2O \qquad (6\text{-}1)$$

$$2\,AlBr_3 + 3\,H_2O \Leftrightarrow Al_2O_3 + 6\,HBr \qquad (6\text{-}2)$$

In order to verify the influence of hydrogen content with a thicker alumina layer on the drift rate, an alumina layer with a thickness of 1000 Å was deposited and the hydrogen was varied according to the procedure described by Arnoux et al. [6,12]. The properties of the formed layers are summarized in table 6-1.

After deposition of the alumina layer, the contact windows for the source, the drain and the substrate had been opened. Simultaneously, the aluminum contacts and several ISFETs gates covered with aluminum, thereby forming the MAOSFETs distributed dispersedly on the wafer, had been performed after the metallization. The last step on the wafer is an anneal under nitrogen at 450 °C during 30 minutes to form low ohmic

contacts. After dicing of the wafer some of the remaining MAOSFET chips had been annealed at 400 °C for 10 minutes under ambient atmosphere [11]. These MAOSFET can then be tested and transformed into ISFET by etching the metal gate with a phosphoric/acetic acid solution at 70 °C, the metal contacts should be protected during the etching.

Table 6-1. *Properties of the alumina layer [6].*

	High H2 content	low H2 content
refractive index	1.75	1.75
growth rate (Å/min)	61	42
pin-hole density (nb/cm^2)	0.4	6.5
grain size (nm)	50	35

The drift of the ISFETs and MAOSFETs fabricated with low H_2 and thicker Al_2O_3 layer were measured with a standard amplifier and the standard measuring conditions [3,11]. The drift rates are counted after 5 hours of operation at the third exposure to the solution .

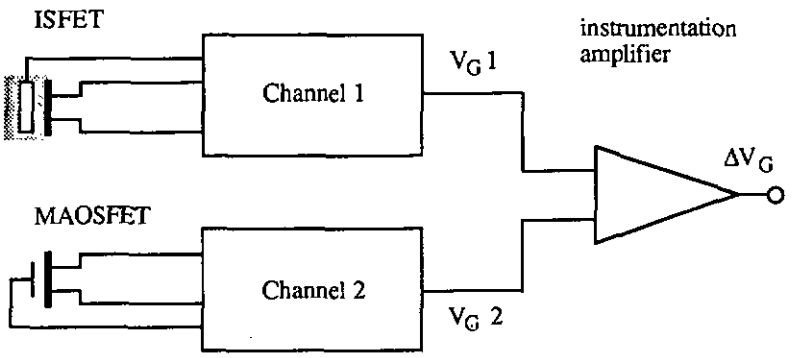

Figure 6-1. *Arrangement of the amplifier for the differential measurements.*

The method using differential pairs reducing the drift rate had been observed. The FET pairs with normal thickness (600 Å) and high hydrogen content of the alumina layer were measured by a special amplifier which operates the ISFET and MAOSFET at a constant drain source voltage and a constant drain source current (V_D = 0.5 V and I_D = 100μA) at 25 °C, in pH 7 buffer solution (MERCK). With this amplifier the drifts of V_G

for individual MAOSFETs and ISFETs can be measured at the same time. The arrangement of the measuring system is illustrated in figure 6-1.

6.4 Results

The long term drifts of an ISFET and of a MAOSFET as well as their differential signals, which were measured at the same time, are shown in figure 6-2.

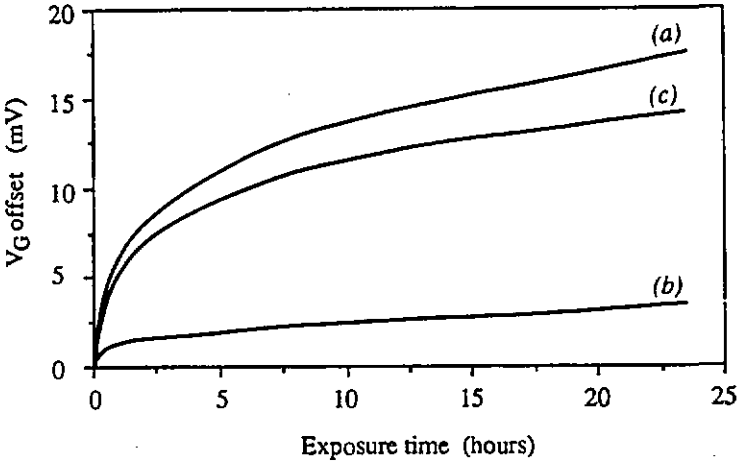

Figure 6-2. *The long term drift af (a) an ISFET, (b) a MAOSFET and (c) the differential measurement of this pair.*

Table 6-2.*The drift rate for ISFETs and MAOSFETs fabricated with low H_2 content after 5 hours af operation.*

normal thickness of the alumina layer (600 Å) [11]		
	ISFETs (n)	MAOSFETs (n)
low H_2	0.28 [mV/h] (12)	0.03 [mV/h] (8)
low H_2 + anneal 400 °C	0.15 [mV/h] (12)	
thicker alumina layer (1000 Å)		
	ISFETs (n)	MAOSFETs (n)
low H_2	0.25 [mV/h] (8)	0.03 [mV/h] (10)
low H_2 + anneal 400 °C	0.08 [mV/h] (6)	0.05 [mV/h] (2)

(n) : number of the FETs measured.

This result shows that long term drift is reduced with differential measurement. In this measurement, we found that the drift rate of the ISFET is higher than that of the MAOSFET for the pairs when the same stabilization time is taken.

This difference in the drift rates between ISFETs and MAOSFETs also appears in other investigations. During studies on reduction of the drift with low hydrogen content and anneal treatment, the ISFETs and MAOSFETs have different drift rates when ISFETs and MAOSFETs are fabricated in an atmosphere of low hydrogen content. The results of these studies are summarized in table 6-2.

6.5 Discussion

The results of the drift rates with only low hydrogen content show an anomalous difference between the ISFETs and the MAOSFETs. According to previous studies the drift of the ISFETs is caused by solid state effects [5,6], the drift behavior of MAOSFETs is the same as for ISFETs. It can be expressed as [10,13]:

$$\frac{\partial V_G}{\partial t} = \frac{\partial Q_{ss}}{\partial t\, C_o} \qquad (6\text{-}3)$$

where Q_{ss} is the charge inside the insulator and C_o is the insulator capacitance per unit area. If the hydrogen content of the alumina only was considered to effect the drift rate, the drift rates of the ISFET and MAOSFET should be similar when the hydrogen content was reduced. Therefore a cause for this difference in drift rates originating in the fabrication procedure has to be considered. It makes a difference of charges inside the insulator between the ISFET and the MAOSFET.

Analyzing every step of the fabrication, a difference between the ISFETs and the MAOSFETs, which are only located in the gates, is found. Before metallization of the gates for the MAOSFETs and contacts of devices, ISFETs and MAOSFETs are identical. After aluminum etching the metal gates of the MAOSFET are formed. In order to obtain good contact between aluminum and silicon, an anneal at 450 °C has to be carried out at the end of the process. This high temperature treatment with and without aluminum gate makes the only difference between the ISFETs and the MAOSFETs. If we look through the results during the reduction procedure, as shown in table 6-2 and combine all results, the very interesting phenomenon that the drift rate changes with H_2 content and anneal steps can be found (table 6-3).

From this table we find that when the hydrogen content is reduced and the normal anneal is performed on MAOSFETs, their drift rate is decreased. This result corresponds to drift measurements on the MAOS capacitor [6,12]. It confirms that the hydrogen in the

alumina layer is mainly responsible for the drift of MAOSFETs. However, the drift rate of the modified ISFETs is still similar to that of normal ISFETs when the hydrogen content is low and a normal anneal is performed. Therefore, this difference of the drift rates between the ISFET and the MAOSFET is assumed to be made by annealing with aluminum over the gate. The results for the ISFET with an additional annealing at 400 °C with the gate area covered by aluminum in table 6-3 confirms this assumption. This result explains that the low H_2 content can reduce the drift rate only together with the aluminum anneal. The surface of the alumina layer is changed by this anneal.

Table 6-3. *The drift rate changes with H_2 content and anneal steps.*

	ISFETs	MAOSFETs
high H_2 normal anneal	x	x
low H_2 normal anneal	x	↓
low H_2 + anneal 400 °C	↓	↓

Legend: x : normal drift rate (0.2- 0.3 mV/h).
↓ : drift rate is reduced.

Based on these results and previous studies, an explanation for drift phenomenons can be obtained. When the hydrogen content is reduced during the fabrication procedure of the ISFET and the MAOSFET, drift caused by bulk polarization due to hydrogen ions in the interstitial position is reduced; however the grain size of the alumina is dependent on the hydrogen content during deposition of the alumina layer, as explained by the properties of alumina layer shown in table 6-1. Lowering hydrogen content results in enlarged grain boundaries in the alumina layer. The drift by migration of other ions along the grain boundaries becomes a major component of the drift now. Therefore the drift rate of the ISFETs without annealing with the gate area covered by aluminum is not reduced. When a normal anneal with aluminum gate is performed on the MAOSFET, the aluminum atoms diffuse into the alumina layer to change the morphology of the alumina grain. The grain boundaries on the surface of the alumina are made narrow. Ion migration along the grain boundaries is prevented, so that the drift rate of the MAOSFET with low hydrogen content is reduced. The drift rate of the ISFETs on which an additional anneal with the gate area covered by aluminum is performed is also reduced.

In addition, a test of the anneal with aluminum on the MAOSFETs and the ISFETs with a high pH content in the Al_2O_3 layer was performed. It was found that the drift rates

can not be reduced. From this result we conclude that the hydrogen content of the alumina is the mainly influencing the drift, at high concentration of hydrogen. The drift rate for the MAOSFETs and the ISFET can therefore not be much improved by an additional anneal for diffusion of aluminum into the alumina layer.

The effect of annealing the ISFETs with a higher temperature (450 °C, 10 min) ($d_{Al_2O_3}$ = 1000 Å with low H_2 content) was also tested. The drift rate is higher than that measured on normal ISFETs. This phenomenon is probably caused by the remaining aluminum ions in the alumina, due to deeper diffusion as a result of the higher temperature.

These results also show that the drift phenomena are caused by the migration of other ions along the grain boundaries localized in a thin layer near the alumina surface. The changes in thickness of the alumina layer do not change the drift rate of the MAOSFET and the ISFET.

6.6 Conclusions

A reduction in the drift rate for the pH sensitive ISFETs with alumina as the pH sensitive layer is realized by decreasing the H_2 content during deposition of the Al_2O_3 layer, followed by an anneal with a layer of aluminum on top of the alumina. This study confirms that the base-line drift of the alumina ISFET is mainly caused by solid state effects of the alumina. It includes two components: (a) the hydrogen trapped in the alumina with γ-structure, where aluminum ions do not completely fill up all the interstitial space during the deposition process of Al_2O_3 layer, and (b) the ion migration along the grain boundaries which are localized near the surface of the alumina layer. The annealing process plays a major role in the diffusion of aluminum.

It has been shown that differential measurement with an ISFET-MAOSFET pair can reduce the drift rate in pH measurements with the pH-ISFETs.

Although the drift rate can be reduced by these methods, the drift effect still remains after 5 hours and a third exposure to the test solution. That is because the different ions diffused into alumina during the fabrication process are polarized in a static electrical field and the control of the ion diffusion is difficult. It still effects the stability of the ISFET. Therefore the changing measurement method from static way to dynamic way, such as the pH measurement method, based on AC temperature modulation of the ISFET, is a possibility to eliminate the drift of the ISFET.

6.7 References

[1]. H.Abe, M. Esashi and T. Matsuo, IEEE Tras. Electron Devices, Vol. ED-26, No. 12, 1979, 1939-1944.

[2]. T. Matsuo and M. Esashi, Sensors and Actuators, Vol. 1, 1981, 77.

[3]. H.H. van den Vlekkert, N.F. de Rooij, Analusis, Vol. 16, No. 2, 1988, 110-119.

[4]. L. Bousse and P. Bergveld, Sensors and Actuators, Vol. 6, 1984, 65-78.

[5]. H.C.G. Ligtenberg, Thesis, University of Twente, The Netherlands, 1987.

[6]. C. Arnoux, Thesis, University of Neuchâtel, Switzerland, 1988.

[7]. P. Balk and F. Stephany, J. electrochem. Soc., Vol. 118, No. 10, 1971, 1634-1638.

[8]. F. Stephany, Thesis, University of Aachen, West Germany, 1979.

[9]. H.H. van den Vlekkert, M. Decroux and N.F. de Rooij, Proc. Transducers'87, Tokyo, Japan, 1987, 730-733.

[10]. H.H. van den Vlekkert, Thesis, University of Neuchâtel, Switzerland, 1988.

[11]. K. Hug, diploma report, University of Neuchâtel, Switzerland, 1989.

[12]. Ch. Arnoux, R. Buser, M. Decroux, H.H. van den Vlekkert and N.F. de Rooij, Proc. Transducers'87, Tokyo, Japan, 1987, 751-754.

[13]. Chapter 5 of this thesis.

Chapter 7
Distribution of ΔV_T of Dual FETs in View of Their Application to Differential Measurements with ISFET-MAOSFET Pairs

published in:

Sensors and Materials, Vol. 2, No. 2, 1990, 67-73

"**Distribution of ΔV_T of Dual FETs in View of Their Application to Differential Measurements with ISFET-MAOSFET Pairs**"

B. Hu, H. H. van den Vlekkert and N. F. de Rooij

CHAPTER 7 Distribution of ΔV_T of Dual FETs in View of Thier Application to Differential Measurements with ISFET-MAOSFET Pairs

7.1 Abstract

A dual FET (ISFET-MAOSFET) using Al_2O_3 on SiO_2 as the gate insulator has been fabricated. The influences of the interfaces between SiO_2 and Al_2O_3, and between Al_2O_3 and the electrolyte solution on the uniformity of the V_T (threshold voltage) for individual FETs and ΔV_T (the difference of the V_T between two FETs of the pair) over a wafer have been studied. The distributions of ΔV_T have shown comparable standard deviations for MOSFET (metal silicon dioxide semiconductor field effect transistor) pairs (31 mV), for the MAOSFET (metal alumina silicon dioxide semiconductor field effect transistor) pairs (29 mV) and for the ISFET-MAOSFET pairs (29 mV). These results have led to the conclusion that the packaging and the Al_2O_3/SiO_2 and liquid/solid interfaces do not change the uniformity of the threshold voltages.

7.2 Introduction

Since the first pH-ISFET was presented [1], many investigations on the pH sensitivity, long-term drift and temperature response of the ISFETs have been carried out. A pH sensitivity of 55mV/pH and a long-term drift of 0.2 mV/hr were measured for the ISFET with Al_2O_3 as a sensitive layer [2]. The temperature response and the long-term drift of the ISFET affect the accuracy of the sensor. Comparison of the results of the long term drift measurements on pH-ISFET and MAOSFET as shown in Figure 7-1, after a period of the stabilization in a buffer solution, the drift on ISFET is similar with the drift on MAOSFET. This can be explained that the effect is mainly due to solid-state effects as shown before [3,4]. A part of the temperature response of ISFET is caused by solid-state effect also. Therefore these effects can be compensated by a differential measurement set up using a MAOSFET and an ISFET [5], as is shown in Figure 7-2. In principle the pH value of the test solution (pHx) can be expressed by [4]:

$$pHx = pHo - \frac{V_T(pHx) - V_T(pHo)}{S} \qquad (7\text{-}1)$$

where pHo is the pH value of the solution in which the ISFET is calibrated, pHx is the pH value of the solution to be determined, $V_T(pHo)$ is the threshold voltage of the ISFET calibrated at pHo, $V_T(pHx)$ is the threshold voltage measured at pHx, and S is the pH sensitivity of the ISFET. S is expressed by [6]:

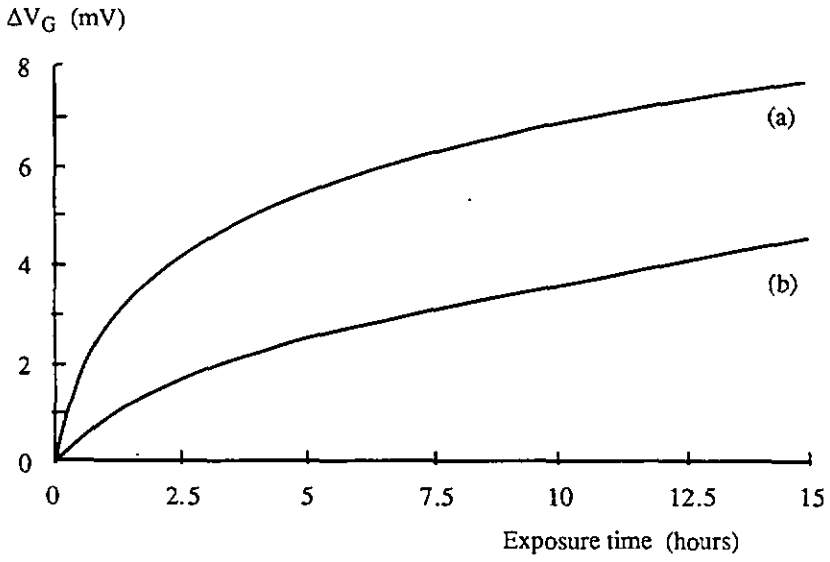

Figure 7-1. *The long term drift measurements on (a) ISFET and (b) MAOSFET.*

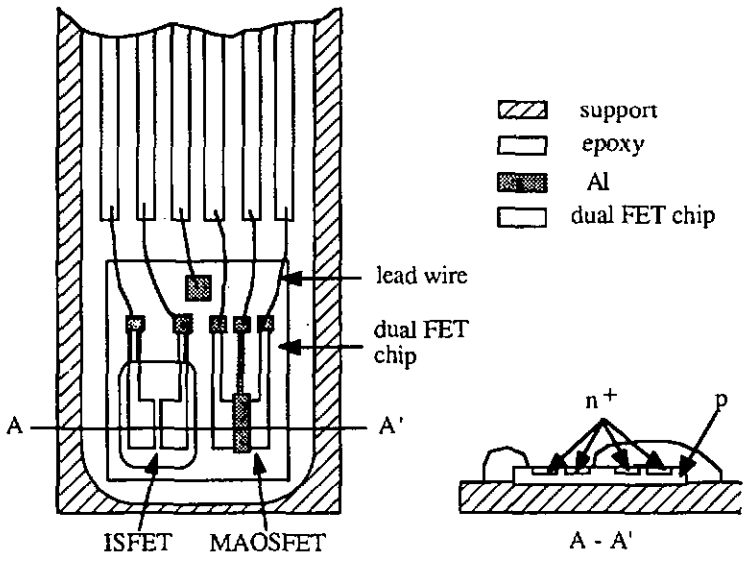

Figure 7-2. *The structure of the pH-sensitive FET pair.*

$$S = \frac{\partial V_T}{\partial pH} = -\frac{\partial \Psi o}{\partial pH} = 2.303 \frac{kT}{q} \frac{\beta}{\beta+1} \qquad (7\text{-}2)$$

where Ψo denotes the potential difference between the insulator surface and the bulk of the solution, k the Boltzmann constant, T the absolute temperature, q the unit charge and ß the sensitivity parameter [6]. Since $V_T(pHo)$ is subjected to drift and temperature effects, the exact value of pHx in (1) is only known immediately after calibration.

When subtracting from the equation (7-1) the threshold voltage of a MAOSFET, which is subjected to drift and temperature effects comparable to those of the ISFET, expression (7-1) can be transformed to:

$$pHx = pHo - \frac{(V_T(pHx)-V_T^{(MAOS)}) - (V_T(pHo)-V_T^{(MAOS)})}{S}$$

$$= pHo - \frac{(\Delta V_T(pHx)-\Delta V_T(pHo))}{S} \qquad (7\text{-}3)$$

where $\Delta V_T(pHx)$ denotes the difference in threshold voltage between the ISFET in a solution with pHx and the MAOSFET,and $\Delta V_T(pHo)$, the difference in threshold voltage between the ISFET in the calibration solution with pHo and the MAOSFET.

If the fabrication process has a good reproducibility of ΔV_T, the drift and temperature effects are eliminated. If ΔV_T were a constant value, calibration would no longer be necessary. In practice however, FET pairs fabricated on the same chip have different ΔV_T's which are not uniformly distributed over the wafer, especially for ISFET/MAOSFET pairs [7]. The nonuniform distributions of surface impurities of the substrate and of charges in the insulator layers are considered to be responsible for these variations. Threshold voltage control introduced by boron ion implantation through the oxide layer for n-channel FETs can make the distribution of surface impurities of the substrate more uniform. In this work, the reproducibility of ΔV_T and the influences of the fabrication process and of the interfaces (SiO_2/Al_2O_3, Al_2O_3/electrolyte solution) on the reproducibility have been investigated.

7.3 Experimental

The ISFETs are operated in constant current mode. The gate-source voltage V_G is measured at a constant drain current I_D of 100 µA and a constant drain-source voltage V_D of 0.5 V. In the linear region, the gate- source voltage is:

$$V_G = \frac{I_D L}{\mu_n W C_i V_D} + V_T + \frac{1}{2}V_D \qquad (7\text{-}4)$$

where μ_n denotes the electron mobility, W the channel width, L the channel length and C_i the insulator capacitance per unit area. Since mainly the term V_T is subject to change, ΔV_T for FET pairs is approximately equal to ΔV_G. Therefore, in all measurements, V_G of the FETs was measured. The ISFET characteristics were measured in a pH7 buffer solution with a Ag/AgCl reference electrode. The MOSFET and MAOSFET characteristics were measured with a needle prober connected to an HP parameter analyzer.

The contribution of dielectric and metallization layers to the gate-source voltage V_G of individual FETs and to ΔV_G of FET pairs was investigated statistically by establishing their distributions over the wafer. Three different FET pairs (FET1-FET2) were fabricated: two MOSFETs, two MAOSFETs and an ISFET-MAOSFET pair. They are shown in Table 7-1 with their successive gate layers.

All wafers were made in the same fabrication run, following identical steps [3], until the last ones which were specific for each device. A SiO_2 layer doped with boron was deposited on a p-type silicon wafer. The windows of source and drain were opened to the silicon and a deposition of the SiO_2 layer doped with phosphorous was made. After the gate areas, which were 15 μm long and 500 μm wide, were opened, an oxidation of 800 Å on the gate areas and the diffusion for the channel stopper, source and drain occurred at the same time. An Al_2O_3 ion-selective layer was deposited for MAOSFETs and ISFETs. They were fabricated on one wafer. All connections and gate regions for MAOSFETs and MOSFETs were then metallized after the contact holes were opened. Two different metal gates for the MOSFET and MAOSFET were formed: one (called the "large" gate) had a contact pad for wire bonding and the other (called the "short" gate) only covered the gate area and had no contact pad. The different gates have been made for previous measurements; they were not relevant to these experiments. The ISFETs were encapsulated on PCB strips with epoxy, leaving only the active parts of the ISFETs exposed to the solution.

In order to test the effect of ion implantation through the gate oxide on the uniformity of the V_G and ΔV_G, after gate oxidation, boron was implanted on one half of each wafer. The other half was protected by photoresist during the implantation.

7.4 Results and Discussion

The V_G measurements for individual FETs and FET pairs are represented by normal distributions. A typical distribution is shown in Figure 7-3 for the case of MAOSFETs without implantation. The mean value and standard deviation (SD) of all MOSFET and MAOSFET measurements are listed in Table 7-2. It is indicated that the

Table 7-1: device matrix: gate layers.

	FET 1	FET 2
(a)	[MOSFET]	[MOSFET]
	Al	Al
	SiO_2	SiO_2
(b)	[MAOSFET]	[MAOSFET]
	Al	Al
	Al_2O_3	Al_2O_3
	SiO_2	SiO_2
(c)	[MAOSFET]	[ISFET]
	Al	
	Al_2O_3	Al_2O_3
	SiO_2	SiO_2

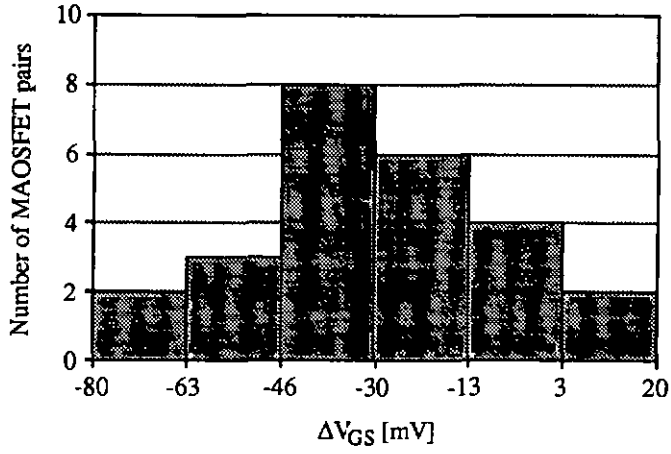

Figure 7-3. *The distribution of the Source-Gate voltage difference (ΔV_G) of MAOSFET pairs without implantation.*

MAOSFET pairs have the same standard deviation of ΔV_G as the MOSFETs. The MOSFETs and MAOSFETs with boron implantation of $2.5 * 10^{11}$ ions/cm^2 show lower

SDs (about 4 mV less) than those without implantation. However, this difference is small compared to the magnitudes of the SDs and thus not statistically relevant.

Table 7-2. *The mean value and the standard deviation of V_G for individual FETs (V_G1 and V_G2) and FET pairs (ΔV_G) of the MOSFET and MAOSFET pairs.*

		V_G1 short (mV)		V_G2 large (mV)		ΔV_G (V_G1-V_G2)	
	n	$\bar{X}$	SD	$\bar{X}$	SD	$\bar{X}$	SD
MOSFET	(28)	1044.1	49.4	1046.4	45.0	-2.3	31.0
MOSFET*	(28)	1784.9	47.9	1777.7	46.9	7.2	27.8
MAOSFET	(32)	684.4	37.4	722.6	36.9	-38.1	28.6
MAOSFET*	(32)	1556.3	69.3	1622.4	67.5	-66.2	23.6

* ion implanted through gate oxide on half part of the wafer (2.5 E11 ions/cm^2 of Boron)

In order to evaluate the measurement error of V_G, 18 measurements were carried out on the same MAOSFET over several days. An error of ± 6 mV was observed. The error was considered to be due to the varying contact resistances of the needle connections. Therefore the sensors were bonded and encapsulated, which allowed reduction of the measurement error to ±1 mV.

The ΔV_G of ISFET-MAOSFET pairs have a standard deviation of 29 mV as shown in Table 7-3. They were measured after bonding and encapsulation. The uniformity is the same as for the MAOSFET pairs. This indicates that there is no influence of the solid/liquid interface on the distribution. The same MAOSFETs (large gate) were used for both the MAOSFET pair measurements (before encapsulation) and for the ISFET-MAOSFET pair measurements (after encapsulation). Although a shift in the mean value of V_G for the MAOSFETs was observed between the two measurements, the standard deviations of individual FETs (V_G) and dual FETs (ΔV_G) were the same (see Table 3). Hence, the packaging does not change the uniformity. From these results we also found that the change of interface from Al/Al_2O_3 to electrolyte-solution/Al_2O_3 does not influence the uniformity of ΔV_G.

Table 7-3. *The mean value and the standard deviation of the measurements for individual FETs (V_G1 and V_G2) and FETs pairs (ΔV_G) of the MAOSFETs and ISFET-MAOSFET pairs.*

		V_G1 short (mV)		V_G2 large (mV)		ΔV_G (V_G1-V_G2)	
	n	$\bar{X}$	SD	$\bar{X}$	SD	$\bar{X}$	SD
MAOSFET	(32)	684.4	37.4	722.6	36.9	-38.1	28.6
IS-MAOSFET	(29)	1727.3	29.7	693.4	37.5	1033.9	29.3

The results discussed above were obtained from devices fabricated in the same batch. The results are not always reproducible between different batches, but the general conclusions remain valid. The lowest observed standard deviations of ΔV_G were 11 mV without implantation and 6.8 mV with implantation. As before, ion implantation improved the uniformity of distribution, and the difference of standard deviation with or without implantation is the same as the results in Table 7-2 (about 4 mV).

7.5 Conclusions

The previously discussed results are summarized in Table 7-4. The following conclusions can be drawn:

1) The deposition of the Al_2O_3 layer on SiO_2 does not change the standard deviation of ΔV_G for FET pairs. The rather high standard deviation for every kind of FET pair is caused by fabrication steps before the deposition of Al_2O_3 layer.
2) The packaging with normal bonding and encapsulation processes reduces the measurement error, but has no significant effect on the distribution of ΔV_G.
3) The uniformity of ΔV_G can be slightly improved by boron implantation.
4) The interface between Al_2O_3 and electrolyte solution does not change the uniformity of ΔV_G.

Therefore the uniformity of ΔV_G is mainly determined by the MOSFET fabrication process. If a pH accuracy of $\pm$ 0.1 pH unit (SD) is required, the SD of ΔV_G should not exceed $\pm$ 5 mV. Cheung et al.[7] demonstrated that the MOSFET fabrication process can be improved so as to meet this specification. In that case only a limited number of dual FET sensors on one wafer shoud be measured in order to determine the average ΔV_G of the wafer, and the other FET pairs can be used without calibration.

Table 7-4. *The collecting measurements of the dual MOSFETs, MAOSFETs and ISFET-MAOSFETs.*

		V_G1 short (mV)		V_G2 large (mV)		ΔV_G (V_G1-V_G2)	
	n	$\bar{X}$	SD	$\bar{X}$	SD	$\bar{X}$	SD
MOSFET	(28)	1044.1	49.4	1046.4	45.0	-2.3	31.0
MOSFET*	(28)	1784.9	47.9	1777.7	46.9	7.2	27.8
MAOSFET	(32)	684.4	37.4	722.6	36.9	-38.1	28.6
MAOSFET*	(32)	1556.3	69.3	1622.4	67.5	-66.2	23.6
IS-MAOSFET	(29)	1727.3	29.7	693.4	37.5	1033.9	29.3

* ion implanted through gate oxide on half part of the wafer.

7.6 References

[1]. P. Bergveld, IEEE Trans. Biomed. Eng., BME-19, (1972), 342-351

[2]. C. Arnoux, B. Kloeck, H. H. van den Vlekkert and N. F. de Rooij, Proc. SSC-ASMT (1985), 37-43, Interlaken, Switzerland.

[3]. H. H. van den Vlekkert and N. F. de Rooij, Analusis, 16 (2), (1988), 110-119.

[4]. H. H. van den Vlekkert, Thesis, University of Neuchâtel in Switzerland, 1989.

[5]. G. H. Wang, D. Yu and Y. L. Wang, Sensors and Actuators, 11 (1987), 221-237.

[6]. L. Bousse, N.F. de Rooij and P. Bergveld, IEEE Trans. Electron Device, Vol. ED-30, No. 10, 1983, 1263-1270.

[7]. P. W. Cheung, S. J. Pace and R. P. Bigliano, Proc. Transducers '87, Tokyo, Japan, June 1987, 742-746.

CHAPTER 8
Conclusions

CHAPTER 8 Conclusions

The packaging and long term drift behavior are two major problems in the applications of the ISFET. In this thesis we have realized a technique, using back-side contacts, which has been actively and effectively used in the packaging of miniaturized biomedical and biochemical sensors. And the drift problems of the pH-ISFET have been improved.

8.1 Fabrication and application of the pH-ISFET with the back-side contacts

In order to realize a possibility to avoid packaging problems, due to the bonding wires and encapsulation, as well as simplifying the packaging process, the pH-ISFET and the combined ISFET/Temperature sensor with back-side contacts have been studied. A simple fabrication technique, etching holes with anisotropic etchent followed by deep diffusion in silicon membranes for the inner cross sections of the contacts, was used. It gave a possibility to glue the electric wires directly into the contact holes on the back side of the sensor chip. It avoided to increase the size of the sensor caused by bonding wires and encapsulation. The sensors had a small size and a smooth surface. The results showed the same characteristics for the pH-ISFET with standard bonding techniques. Using this contacts technique the sensor was used in measurements of interdental plaque pH, where the sensor was mounted into a human enamel piece flush with the surface, and a pH-ISFET was integrated with a pressure sensor.

A very important and very useful application of the pH sensor is using it as an internal pH sensing element for a gas sensor based on the Severinghaus principle [1]. A study of the implementation of the pH-ISFET with back-side contacts, in place of the glass electrode in a traditional CO_2 gas sensor has been presented. A good sensitivity of 56 mV/log(Pco_2) was found. Using back-side contacts on the pH-ISFET the packaging of the sensor was simplified and the active surface of the ISFET could be placed much closer to the gas permeable membrane of the sensor. It resulted in a faster response time and a fast temperature response time. The sensor could be made very small without the effect of increasing the impedance and response time associated with the reduced size, that is apparent in the case of gas sensors with a glass electrode as pH sensitive element. This study can also be extended to other kinds of the gas sensors based on the Severinghaus principle, by changing the inner electrolyte solution and the gas permeable membrane.

8.2 Reducing the drift rate of the pH-ISFET

The pH-ISFETs, with Al_2O_3 as a pH sensitive material have a long term drift of 0.2-0.3 mV/h after a stabilization time of 5 hours. In cases that require a high accuracy, this stability is not acceptable. In this thesis two method to reduce the drift rate were considered: in the fabrication process and in the measuring mechanism. With these different methods the drift rate was reduced drastically.

In their fabrication process we found that the drift rate was reduced by decreasing the H_2 content during deposition of the Al_2O_3 layer, followed by an anneal with a layer of aluminum on top of the alumina. A drift of less than 0.1 mV/h after a stabilization of 5 hours was obtained. With the results of this study we concluded that the drift of the alumina ISFET is mainly caused by the hydrogen trapped in the alumina with γ-structure, where aluminum ions do not completely fill up all the interstitial space during the deposition process of the Al_2O_3 layer, and the ion migration along the grain boundaries which are localized near the surface of the alumina layer. The annealing process plays a major role in the diffusion of the aluminum. Such results are first obtained directly on the ISFET.

The results of the drift measurements on the ISFETs and MAOSFETs have shown that the anneal temperature has an effect on the drift rate and that the drift rate of the ISFET is not always the same as that of the MAOSFET, it was often higher than that of the MAOSFET. This can be considered as a result of the diffusion of the aluminum in the Al_2O_3 layer. In order to control this diffusion we propose an investigation into the concentration of aluminum and the depth of the diffusion layer in the Al_2O_3 layer, as well as effective diffusion methods such as ion implantation.

Until now, even we have a good control of the diffusion of aluminum into alumina layer, the drift of the ISFET can not be eliminated completely. In the first hours of the measurement the drift behavior of the ISFET is still one problem in its applications. It can be considered that it is a problem of the ISFET measurement with the static method.

A novel pH measurement technique with pH-ISFETs has been presented. It shows us a dynamic measurement technique. For improving the drift of the ISFET it is much better than the static measurement method. The sensor consists of an ISFET, a heating resistor and a temperature sensing diode. The temperature of the device was modulated, and the derivative of the ISFET response with respect to the temperature was detected directly on the ISFET signal. This temperature modulation of the ISFET was sensitive to the pH. When the temperature dependence of the measured solution was taken into account, a surface sensitivity of 0.21 mV/°CpH was obtained, in good agreement with expected value of the surface investigated. Using the new method, the influence of long term drift can be reduced. The modulation temperature measurement mechanism shows

clear evidence for the solid state origin of the drift of the ISFET with the alumina sensitive layer. With a smaller temperature gradient between the ISFET and the solution, this new technique seems to be very suitable for the characterization of the sensing surface of an ISFET. Application to the study on the surface ionization enthalpies of the materials are possible. To achieve this, a Peltier element has to be integrated within the device to generate temperature oscillations without any shift between the mean temperature of the solution and the mean temperature of the device. Since this method is based on the temperature characteristics of the ISFET, the temperature of the sample directly effects on the amplitude of the temperature modulation signal and the measurement results. In this study, the temperature of the device and the modulating variation of the temperature were measured by a diode, and the temperature of the sample and the modulation temperature variation were kept at constant (25 °C and 1 °C). But in the applications the temperature condition of the measurements is not always constant. We need to improve this method and to develop a compensating system for the changes of the temperature.

The pH differential measurement with an ISFET-MAOSFET pair was used to reduce the drift effect since the solid state effects were responsible for the drift of the ISFET. Since the drift was reduced, an ideal device would not require calibration, if ΔV_T could be controlled and made constant. Therefore the influence on the uniformity of the V_T and ΔV_T for the ISFET and MAOSFET was studied. The uniformity of the ΔV_T is mainly determined by the MOSFET fabrication process.

Summary

Since the first ISFET (Ion Sensitive Field Effect Transistors) was presented in 1970 by Bergveld, the pH-ISFETs with alumina as pH sensitive material have been largely improved in their performance. However, some problems still impede the applications of the ISFET especially in the biomedical fields. Example of the problems in the miniaturization of the sensors are the packaging and the baseline drift of the ISFETs.

In order to overcome these problems, a special encapsulation and bonding technique is presented in chapter 3. There the contacts are fabricated on the back side of the chip and the electrical connection wires can be connected directly onto these contacts for making a probe which has as small a diameter as possible after bonding and encapsulation. Furthermore a combined pH/temperature sensor with the above mentioned contact technique is proposed. Following this investigation of the pH-ISFET with back-side contacts, a novel carbon dioxide sensing electrode based on the Severinghaus principle has been developed, which is presented in chapter 4. In this electrode a pH-ISFET with back-side contacts is used as an internal pH sensing element and a temperature sensitive diode is integrated on the same chip, a Ag/AgCl wire is used as a reference electrode. The realization of such an electrode enlarges ISFETs field of the application and shows a possibility to miniaturize such gas sensors.

Another major problem of pH-ISFETs is their long term drift behavior. A novel measurement technique is presented in this thesis by which the pH response of the sensor signal can be separated from solid-state effects that are responsible for its long term drift. In this method, the temperature of the device is modulated at a frequency of 0.5 Hz with a typical amplitude of 1°C. A synchronous detection of the signal of the ISFET gives directly the derivative of the ISFET response with respect to the temperature. When the pH temperature dependence of the measured solution is taken into account, a surface sensitivity of 0.21mV/°C/pH is obtained. This method seems to be very suitable for characterization of the sensing surface of an ISFET and for studying the surface ionization enthalpies of materials.

In chapter 6 the drift behavior is further discussed and different methods of reducing the drift rate of the pH-ISFET with alumina as the pH sensitive material are proposed. It is confirmed that the base-line drift of the ISFET is mainly caused by solid state effects due to the alumina layer. The bulk polarization due to H^+ ions in the interstitial position of the γ-Al_2O_3 structure and the slight ion migration along grain boundaries causing the drift is found by the measurements on the ISFETs and MAOSFETs. When the hydrogen content is reduced, the ion migration along grain

boundaries becomes a major effect on the drift. It indicated an equal or higher drift rate for an ISFET with low hydrogen content than the ISFET with high hydrogen content. This problem can be solved by the diffusion of aluminum into the alumina layer during an annealing procedure. After these studies a conclusion could be obtained that the drift caused by ion migration along the grain boundaries is localized in a thin layer near the alumina surface.

In chapter 7 the influences of the interfaces between SiO_2 and Al_2O_3, and between Al_2O_3 and the electrolyte solution on the uniformity of the V_T (threshold voltage) for individual FETs, and ΔV_T (the difference of the V_T between paired ISFET and MAOSFET) over a wafer is discussed, in order to improve the drift effect with differential measurement and to study the necessity of calibration.

Acknowledgements

In the course of this thesis work I have received highly appreciated help from the insight, knowledge, experience and practical skill of many people. Thanks I owe to:

Professor N. de Rooij, for providing me with the opportunity to study for this Ph. D in his group, and for his support and guidance during this work;

Dr. M. Decroux of the institute of Physics (University of Genève), for his decisive contribution to and guidance during the study of the reduction of the drift of the ISFET with the temperature modulation technique;

Dr. H. van den Vlekkert, who introduced me to the wafer processing techniques at the beginning of this work, as well as contributing to some subjects of this work;

Mr. S. Jeanneret, Dr. G.-A. Racine, Mr. D. Prongué and Mr. K. Hug, for their decisive contribution to certain subject areas and their help during this work;

Mr. G. Mondin of the Centre Suisse d'Electronique et de Microtechnique (Neuchâtel), for the deposition of thin metal films and alumina film;

Ms. S. Pochon for wire bonding;

All my colleagues of the Sensors and Actuators Group of the Institute of Microtechnology of Neuchâtel;

Dr. M. Koudelka, Dr. B. van den Schoot, Dr. B. Kleock and Dr. P. Gimmel of University of Tübingen (Germany) for reading and discussing manuscript;0

Mr. M. Lyons of ASCOM Microelectronics (Bevaix) and Dr. P. Lösel of the Institute of Zoology (Neuchâtel) for their English corrections.

All secretaries of the Institute of Microtechnology for their help.

Further I thank Prof. P. Bergveld, Prof. A. Shah and Dr. M. Decroux for very kindly agreeing to be co-examiners.

I thank Dr. Ye Pei-jian who finished his Ph.D in the Institute of the Microtechnology for his help to contact with prof. de Rooij and for making this thesis possible.